IEEE Access
Multidisciplinary ⋮ Rapid Review ⋮ Open Access Journal

Received January 16, 2021, accepted February 4, 2021, date of publication February 8, 2021, date of current version February 23, 2021.

Digital Object Identifier 10.1109/ACCESS.2021.3057788

Prospects and Challenges of the Hyperloop Transportation System: A Systematic Technology Review

JONAS KRISTIANSEN NØLAND, (Member, IEEE)
Department of Electric Power Engineering, Norwegian University of Science and Technology (NTNU), 7034 Trondheim, Norway
e-mail: jonas.k.noland@ntnu.no

This work was supported by the Open Access internal funding granted by the Norwegian University of Science and Technology (NTNU).

ABSTRACT The present article outlines the core technologies needed to realize the Hyperloop transportation system (HTS). Currently, the HTS vacuum tube train concept is viewed as the fastest way to cross the earth's surface. However, the concept has not yet been demonstrated for subsonic or near-sonic speeds in large-scale implementations. Among the challenging technical areas are the tube's depressurization, the capsule's air resistance, and choked flows occurring around the capsule. There is also a need for effective levitation and propulsion solutions compatible with the velocities being proposed. Moreover, several conflicting objectives have been identified in the HTS design. It is highlighted that the tubes should be wide enough to lower the capsule's drag forces but that a large-sized tube comes at the expense of higher operational energy costs and infrastructure investments. Another struggle is aiming at a low-cost passive track design and, and at the same time, a lightweight vehicle. One technical path is to turn the whole guideway into an electric propulsor, arriving at a 'lightweight capsule solution' (LCS). Alternatively, the vehicle could be transformed into a 'modified airplane' that stores massive amounts of onboard energy, yielding an energy-autonomous 'low infrastructure solution' (LIS). In a case study, it is shown that even LIS technology is compatible with short-haul flights (1500 km) but that it requires an energy reservoir of about 30% of the capsule's overall mass. Results and discussions presented in this paper are supported by analytical predictions with parameters or input data either supported by referred simulations or experiments. In general, the paper aims to open up the discussion, provide a sufficient understanding of the Hyperloop field's multidisciplinary aspects, and establish a foundation for further investigations. In the end, new research tasks have been defined, which have the potential to go beyond the state of current knowledge.

INDEX TERMS Hyperloop, vacuum systems, aerodynamic drag, linear motors, electric propulsion, magnetic levitation, EMS, EDS, EDW, SP-type LIM, SP-type LRM, LP-type LIM, LP-type LSM.

I. INTRODUCTION

The idea of near-sonic ground travel has been an idea for over a century. Already decades ago, the design of a partially evacuated tube was patented to reduce air drag resistance [1]–[3]. In 2013, the idea of 'vactrains' got its rebirth in a white paper, where they got rebranded as the Hyperloop concept [4] and called out as the fifth mode of transportation. The Hyperloop transportation system (HTS) describes passenger capsules moving inside a tube of a low-drag low-pressure environment (i.e., as low as one-thousand of the atmospheric pressure). They are then being propelled and guided by a track inside [5], [6], with a potential of moving near the speed of sound (i.e., near-sonic velocities). In the original concept, air bearings were proposed for levitation, and track-integrated coils were considered for propulsion. The guideway was imagined to be energized with distributed acceleration spots to reduce the infrastructure (covering just a small fraction of the track) [4], [7].

Fig. 1 depicts a brief overview of the generic HTS concept, where passenger capsules constantly move between two stations. As seen, there is an acceleration and de-acceleration time needed (e.g., 0.1 G or 0.2 G acceleration), which restricts HTS to longer distances travel only. Either the capsule floats on its suspension mechanism, or it hangs underneath, as depicted in Fig. 2.

The associate editor coordinating the review of this manuscript and approving it for publication was Kan Liu.

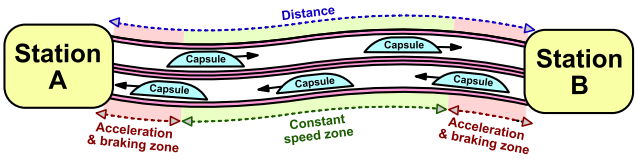

FIGURE 1. Sketch of a conceptual HTS diagram depicting passenger capsules' movement inside a two-way tunnel with two predetermined point-to-point stations. Cruising, acceleration, and braking zones are highlighted (adapted from [8]).

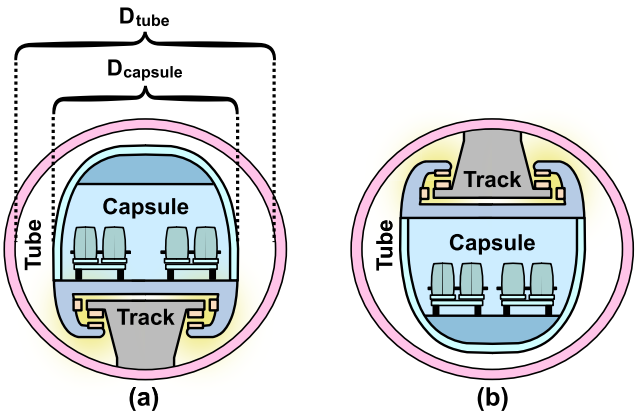

FIGURE 2. Generic illustration of the HTS concept, including the tube, the capsule, and a wide track (seen perpendicular to the moving direction). The tube's inner diameter and the capsule's outer diameter are also indicated. a) Vehicle floats on the track. b) Vehicle hangs underneath the track.

The HTS concept is currently viewed as a promising alternative to short-haul flights, where it can promise less travel time and lower fuel consumption per passenger revenue kilometer (RPK). This is illustrated in Fig. 3, where an energy consumption metric (i.e., drag-to-lift ratio) is used to compare different transportation alternatives. The performances are assessed against the rolling magnetic drag of the electro-dynamic suspension (EDS) system proposed for the Hyperloop, in either simple or more advanced implementations. An excellent characteristic of the magnetic levitation technology is that the ratio between the drag and the lift goes down at higher cruising speeds, which are completely contrary to bullet trains and aircraft propulsion that are subjected to increased air resistance. In order to highlight the best possible potential for the projected low energy consumption of the HTS, the air resistance was assumed to be zero in Fig. 3 (depends on the pressure of the tube and the aerodynamic performance). The realism and challenges of satisfying this assumption are further explored in Section II.

A comprehensive subsonic or near-sonic HTS solution has not yet been designed, built, optimized, or tested. Moreover, the research literature demonstrating magnetic levitation and electric propulsion technologies is currently immature for this speed range, where only a few preliminary studies have been presented to address it so far [8], [9], [12]–[14]. According to a 2018 UK innovation report, the critical short-term research and development needs are on the propulsion, levitation, energy storage, and thermal management system [15]. There is also a need to develop testing facilities, including the tube infrastructure design, and develop an understanding of advanced aerodynamic phenomena occurring inside the tube [16]–[18].

In the field of electromagnetism, the classical maglev technology has been studied for half a century already [19], [20]. However, maglev has been limited in speed due to the presence of atmospheric air pressure. The partially evacuated tube is the only proposed way to reach sub-sonic (≈1000 km/h) or near-sonic (≈1225 km/h) transportation speeds at the surface of the earth.

This paper presents the technology fundamentals of the Hyperloop concept, as well as the proposed technical solutions for propulsion and levitation. A qualitative and quantitative framework is outlined in order to access and investigate different aspects of the Hyperloop. The HTS is still quite new with many uncertainties. Therefore, the paper defends its technological predictions relying on either well-founded theoretical assumptions, analytical formulations, numerical simulations, or experimental validations. It is important to note that the technology's aerodynamic features rely mostly on evidence supported by computational fluid dynamics (CFD). Moreover, the electrical propulsion technologies investigated are supported by finite element analysis (FEA). The paper also provides a comprehensive literature review, which is the first to establish an overall view of the HTS's sub-fields.

The structure of the article is as follows. In Section II, the aerodynamic technology fundamentals of the Hyperloop technology are outlined, including the depressurization of the tube. Then, the proposed suspension methods for the technology are presented in Section III. Moreover, section IV describes the electric propulsion technologies suitable for HTS. Finally, performance investigations of complete technical solutions are analyzed and discussed in Section V before the paper's outline is discussed and concluded in Sections VI and VII, respectively.

II. HYPERLOOP TECHNOLOGY FUNDAMENTALS

This section is dedicated to the core physical principles of the HTS. The Hyperloop concept's main advantage is the opportunity to achieve a high-altitude low-pressure environment at the surface of the earth. In reality, airplanes have to consume vast amounts of energy to get to the altitude where the pressure level is 75 % lower. On the contrary, the Hyperloop is aimed at achieving 99.0 % to 99.9 % lower pressure by recreating the atmosphere experienced in outer space, using an outstretched vacuum chamber. In this section, standard equations, constitutive relations, and natural laws are expressed and applied with technically feasible physical assumptions for the Hyperloop concept. The contribution lies in applying realistic parameters (from referred simulations or experiments) and input data to provide preliminary results and insights on the HTS. The potential of dramatically reducing the capsule's aerodynamic drag is investigated in the three next subsections before the section ends with some consequences on the tube's operational requirements.

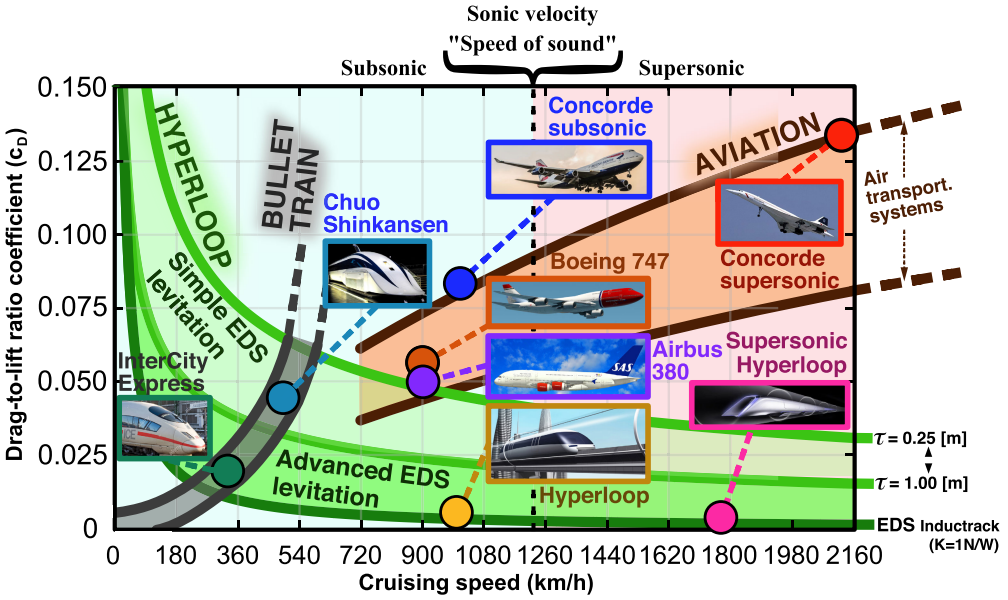

FIGURE 3. Potential for reducing the Hyperloop transportation concept's drag-to-lift ratio at higher speeds, assessed against the conventional rail, classic aviation, and 'Concorde' aviation [extending Fig. 10 of [9] based on the simple EDS eq. (31) and the 'Inductrack' eq. (41)]. The simple levitation concept assumes the most low-cost infrastructure (i.e., track made of aluminum beams). The advanced levitation calculation is based on [10], [11], i.e., a passive ladder-type track (assuming a basic performance of 1 N/W in the lift per drag power). For simplicity, the aerodynamic drag is neglected for the Hyperloop calculations.

A. REDUCED AIR RESISTANCE

The aerodynamic resistance an object experiences when penetrating air is depending on its density. According to the ideal gas law (i.e., standard gas state equation), the density of air (ρ) is directly proportional to the pressure (p), where

$$\rho = \frac{1}{RT}p. \tag{1}$$

The temperature (T) and the pressure (p) is given the in SI units K and Pa, respectively. Moreover, the specific gas constant (R) is approximately 287.05 [m^3Pa/kgK]. It is evident from eq. (1) that the density of air is reduced by lowering the pressure. It implies that reducing the pressure to one-thousand of the atmospheric pressure will reduce the air density with the same amount. Besides, eq. (1) shows that heat accumulated by air in a closed environment resulting in a higher temperature has a positive effect on reducing the aerodynamic drag of moving bodies. For the HTS system, a reasonable assumption might be that the tube temperatures vary between 0 °C (273.15 K) and 40 °C (313.15 K), but can be monitored by the environmental control system, even though variations along the tube will occur. The air resistance that the Hyperloop capsule experience is proportional to the dynamic pressure (p_{dyn}) it is generating according to

$$p_{dyn} = \frac{1}{2}\rho v^2, \tag{2}$$

where v is the capsule's cruising speed. This pressure will act at the front of the capsule and thus, create a drag force. The resisting force is proportional to the capsule's frontal surface area (A_{caps}), but it will also depend on the frontal shape. This effect is taken into account by a dimensionless quantity called the drag coefficient (C_d). It captures the aerodynamic effects related to the geometry and orientation of the object. Usually, it is estimated from computational fluid dynamics (CFD) or measured in experiments. The drag can be formulated as

$$F_{aero} = C_d A_{caps} p_{dyn}, \tag{3}$$

or

$$F_{aero} = \frac{1}{2}C_d A_{caps}\rho v^2, \tag{4}$$

if one inserts for the dynamic pressure. The drag equation predicts that the total drag experienced by a body submerged in air is proportional to p_{dyn}, A_{caps} and C_d. By assuming a constant temperature, the drag's dependency on the pressure can be formulated as

$$F_{aero} = \frac{1}{2}C_d A_{caps} \underbrace{\left(\rho_{atm}\frac{p_{tube}}{p_{atm}}\right)}_{\rho_{tube}} v^2, \tag{5}$$

taking eq. (1) into account. As the drag increase is proportional to the square of v, the maximum achievable speed will be limited unless the tube pressure (p_{tube}) is significantly reduced with respect to the atmospheric pressure (p_{atm}) outside. The effect of a constrained low-pressure environment becomes even more significant when calculating the aerodynamic power (P_{aero}) needed to sustain the cruising speed (v), which is proportional to both F_{aero} and v as follows.

$$P_{aero} = F_{aero}v = \frac{1}{2}C_d A_{caps}\left(\rho_{atm}\frac{p_{tube}}{p_{atm}}\right)v^3. \tag{6}$$

As an example, eq. (6) predicts that if the pressure is one-tenth, one could reach 2.15 times higher speed at the same power consumption (given that C_d is unchanged).

B. THE KANTROWITZ LIMIT

The premise for a low air resistance relies on a low drag coefficient (C_d) inside the tube. This only holds if the tube volume surrounding the capsule can be assumed infinitely large relative to the vehicle. Normally, the walls of the tube are much closer to the capsule. Inevitably, we are dealing with an internal aerodynamic problem, where a violation of the so-called Kantrowitz limit could increase the drag and deteriorate the Hyperloop concept's main benefits. The cross-sectional diameters used to calculate the tube and capsule areas (A_{caps} and A_{tube}) are depicted in Fig. 2. The area ratio of these values indicate the fraction of the tube that are been occupied by the capsule, which is referred to as the blockage ratio

$$\beta = \frac{A_{caps}}{A_{tube}} = \frac{\frac{1}{4}\pi D_{caps}^2}{\frac{1}{4}\pi D_{tube}^2} = \frac{D_{caps}^2}{D_{tube}^2}. \tag{7}$$

Fig. 2 highlights the fact that the tube-capsule arrangement resembles a subsonic or near-sonic wind tunnel, where choked flows and shock waves at the capsule's tail easily occur. The flow around the capsule will accelerate as the bypass area reduces (i.e., high blockage ratio). In these cases, the sides of the capsule are close to the tube. The Kantrowitz limit can be formulated as (profile presented in [16])

$$\frac{1}{1-\beta} = \frac{1}{\mathrm{Ma}}\left(\frac{1+\left[\frac{\gamma-1}{2}\right]\mathrm{Ma}^2}{1+\left[\frac{\gamma-1}{2}\right]}\right)^{\frac{\gamma+1}{2(\gamma-1)}}, \tag{8}$$

where Ma is the mach number ratio relating the cruising speed v to the speed of sound (≈ 1225 km/h) and γ is the isentropic expansion (≈ 1.4). Fig. 4 depicts the Kantrowitz limit, which is a combination of blockage ratio and speed, governed by eqs. (7) and (8). At the speed of sound, a zero blockage is required to avoid choking and prevent the Kantrowitz limit (i.e., infinitely large tube volume). It is evident that for high service speeds, it is virtually impossible to avoid choking air. However, it is important to reduce the violation of the Katrowitz limit, to keep the aerodynamic drag as low as possible.

C. REALISTIC DRAG COEFFICIENTS

From the considerations made so far, it is important to assess how the drag coefficient is affected when choking flows occur. The calculation of the drag coefficient is made using

$$C_d = \frac{2F_{aero}}{A_{caps}\frac{p_{tube}}{p_{atm}}\rho_{atm}v^2}, \tag{9}$$

which is a reformulation of eq. (5). If F_{aero} is found from an experiment or a CFD simulation, C_d can be found from eq. (9). The speed-dependent C_d is in Fig. 5 depicted for several cases. The Hyperloop Alpha [4] report did not present

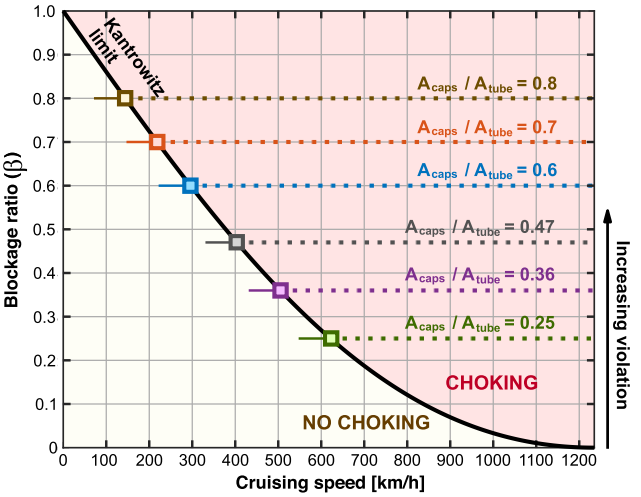

FIGURE 4. The Kantrowitz limit is plotted as a function of blockage ratio (A_{caps}/A_{tube}) and cruise speed. Different area ratios are highlighted, indicating their transition violating the limit. The profile is calculated from combining eqs. (7) and (8), and the figure is adapted from [16].

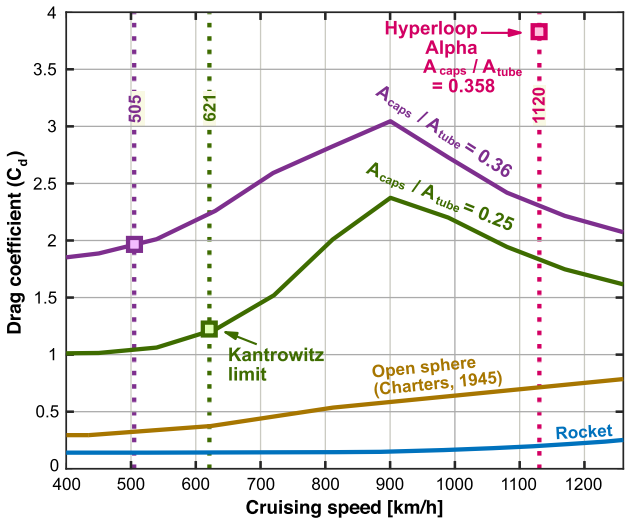

FIGURE 5. The effect of low capsule blockage ratios (A_{caps}/A_{tube}) on the drag coefficient (C_d) as a function of cruising speed (v). The plotted profiles are calculated using eq. (9) with simulation or experimental data taken from [17], [21], [22]. The drag (F_{aero}) was calculated with a tube where $p_{tube} = 101.325$ Pa, i.e., 0.1% of the sea-level, and $T = 15$ °C. The diameter of the capsule (D_{caps}) was 3 m in [17], i.e., $A_{caps} \approx 7.07$ m^2.

any solid background calculations, and is shown to be far off when comparing it with CFD presented in [17], where the numerical model was validated against experiments [21]. For a capsule of blockage ratios 25 % and 36 % at 1000 km/h, the C_d is about 13 and 16 times higher than a rocket moving in free air, respectively. If the increased drag due to higher C_d get too influential, it will inevitably cancel the reduced drag due to the low-pressure environment. This is even more evident in Fig. 6, where the drag coefficient for high blockage ratios (β) of 60 %, 70 %, and 80 %, respectively, are depicted. The choking is shown to start at much lower cruising speeds, when a small tube volume is chosen [as predicted by eq. (8)].

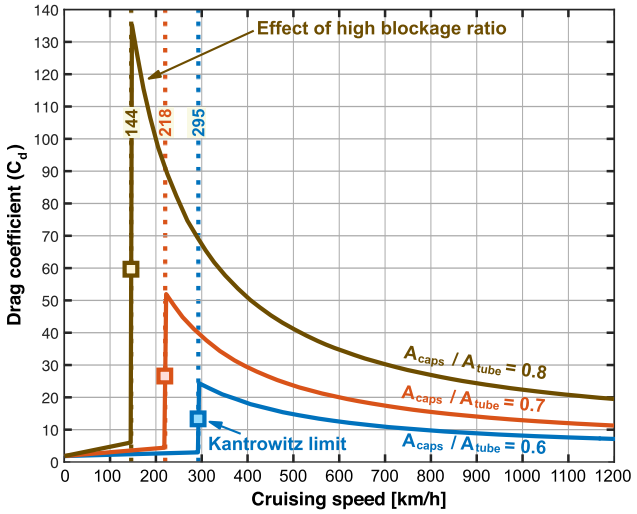

FIGURE 6. The effect of high capsule blockage ratios (A_{caps}/A_{tube}) on the drag coefficient (C_d) as a function of cruising speed (v). The plotted profiles are calculated using eq. (9) with simulation model taken from [18], with associated data in [23]. The drag (F_{aero}) was calculated with a tube where p_{tube} = 100.000 Pa, i.e., 0.0987% of the sea-level, and T = 15 °C. The diameter of the capsule (D_{caps}) was 3.4 m in [18], i.e., $A_{caps} \approx 9.08$ m^2.

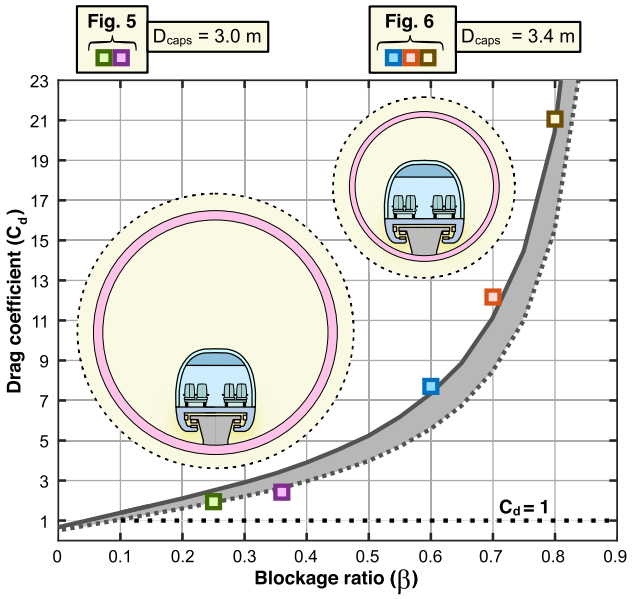

FIGURE 7. The drag coefficient (C_d) projected as a function of blockage ratio (A_{caps}/A_{tube}) at 1080 km/h service speed. The curves plotted in Figs. 5 and 6 are plotted as points, representing their drag coefficient at 1080 km/h.

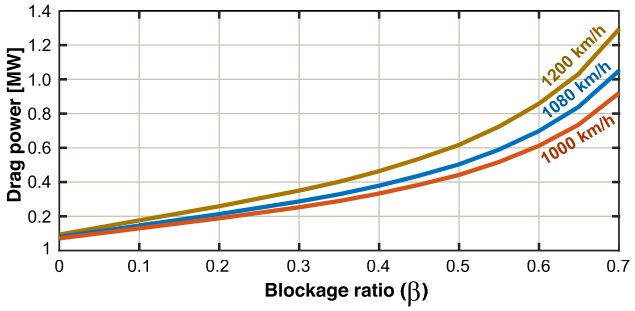

FIGURE 8. Drag power consumption projected curves as a function of blockage ratio (A_{caps}/A_{tube}) for a capsule with diameter D_{caps} = 2.7 m, based on curves given in Figs. 5 and 6. Considered service speeds (v) are 1000 km/h, 1080 km/h, and 1200 km/h.

The most interesting part of the drag profile is the behavior at the cruising speed, where most of the energy consumption occurs for the Hyperloop capsule. The drag coefficient at 1080 km/h (i.e., a relevant service speed) is projected as a function of the blockage ratio in Fig. 7, where the curves are fitted against Figs. 5 and 6. The same data are used to estimate the drag power consumption of a relatively large Hyperloop capsule dimensioned for 50 passengers (PAX), with an outer diameter of 2.7 m [23]. This case is investigated for three different cruising speeds in Fig. 8. For blockage ratios below 0.5, the power consumption flattens out ($\leq$0.5 MW for 1000 km/h), causing a less steep reduction by further increasing the tube size (i.e., lower blockage). This power consumption inevitably represents an optimization problem. This is because a larger tube causes higher operational power consumption to depressurize the tube and more infrastructure costs. This is the issue addressed in the next subsection.

D. OPERATION OF TUBE INFRASTRUCTURE

This subsection will give initial estimates on increasing the tube size (i.e., lowering the blockage ratio) and how it impacts the operational energy consumption. This is studied for the complete depressurization and the additional needs for air leakage compensation. In general, the considerations and calculations are based on the cross-sectional sketch of the tube in Fig. 9 (other key parameters are also stated). In constructing the tube, either steel or concrete are good candidates as the wall material. Even though steel is considered more airtight, it is prone to corrosion. There are early stages of concrete development combined with glass-fiber or carbon-fiber to increase its strength and cope with some of the concrete's inherent weaknesses. The tube structure also has to be supported by pillars connected to the earth's surface, but this part is omitted in the operational infrastructure analysis. We will first work out the tube energizing process before the leakage compensation is being studied as well.

1) TUBE ENERGIZING AND PRESSURIZING

The volumetric continuity equation for the pressure inside of the evacuated tube (p_{tube}) released from the atmospheric condition (p_{atm}) is governed by the pumping speed out of the tube ($\dot{V}_{tube}$) and the tube volume (V_{tube}) as follows [24], [25].

$$V_{tube}\frac{dp_{tube}}{dt} = -\dot{V}_{tube}p_{tube} \tag{10}$$

With the initial condition $p_{tube}(t = 0) = p_{atm}$, the solution the the state equation is

$$p_{tube}(t) = p_{atm}\mathrm{e}^{-\frac{-\dot{V}_{tube}}{V_{tube}}t}. \tag{11}$$

Eq. (11) describes an exponential decay of the pressure if the flow rate of air is constant out of the tube (i.e., m^3/s), referred

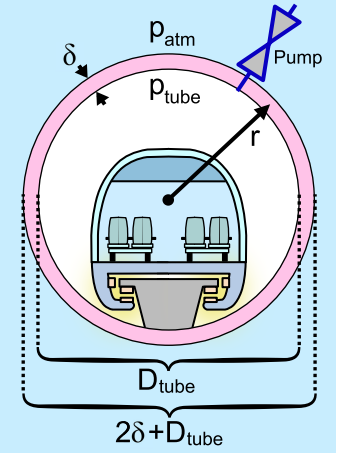

FIGURE 9. Sketch depicting the main geometrical parameters determining the performance of the evacuation system. The pressure inside the tube (p_{tube}) is evacuated by a tube wall of thickness δ. The pump depicted has a nominal power rating of P_{pump}. It is responsible for tube depressurization, as well as compensating for air leakages under operation. The number of pumps is N_{pump}, and they are uniformly distributed along the tube trajectory.

at the high-pressure atmospheric side. When the desired pressure is reached ($t = \Delta t_{tube}$), the time to depressurize the tube (Δt_{tube}) can be formulated

$$\Delta t_{tube} = \frac{V_{tube}}{\dot{V}_{tube}} \ln\left(\frac{p_{atm}}{p_{tube}}\right) = \frac{\pi\left(\frac{D_{tube}}{2}\right)^2 l_{tube}}{N_{pump}\dot{V}_{pump}} \ln\left(\frac{p_{atm}}{p_{tube}}\right). \tag{12}$$

Eq. (12) can be expressed in a way that makes number of pumps per length (N_{pump}/l_{tube}) as an input.

$$\Delta t_{tube} = \frac{\pi\left(\frac{D_{tube}}{2}\right)^2}{\left(\frac{N_{pump}}{l_{tube}}\right)\dot{V}_{pump}} \ln\left(\frac{p_{atm}}{p_{tube}}\right) \tag{13}$$

The total amount of energy needed to depressurize the tube (E_{tube}) are then

$$E_{tube} = P_{tube}\Delta t_{tube} = \underbrace{\left(\frac{N_{pump}}{l_{tube}}\right) l_{tube}}_{N_{pump}} P_{pump}\Delta t_{tube}, \tag{14}$$

where (P_{pump}) is the pumping power needed of each pump during the depressurization process (Δt_{tube}). Eq. (14) can be combined with eq. (13), to make the formulation independent of number of pumps as follows.

$$E_{tube} = \underbrace{\pi\left(\frac{D_{tube}}{2}\right)^2 l_{tube}}_{V_{tube}} \frac{\ln\left(\frac{p_{atm}}{p_{tube}}\right)}{\left(\frac{\dot{V}_{pump}}{P_{pump}}\right)}, \tag{15}$$

In eq. (15), the depressurization energy (E_{tube}) needed is proportional to the volume of the tube (V_{tube}), the ratio between the pump power and the pump flow rate (V_{pump}/P_{pump}, included in the vacuum pump specification), and the natural logarithm of the ratio between the atmospheric pressure

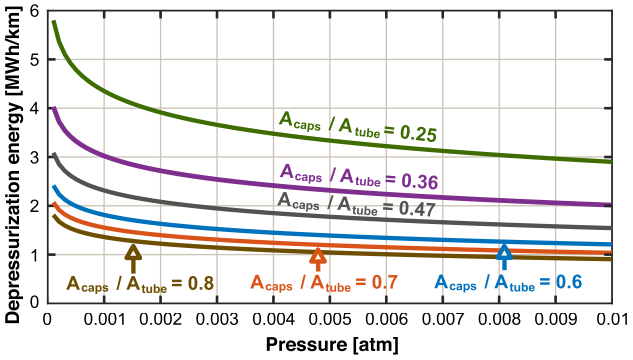

FIGURE 10. Depressurization energy consumption as a function of tube pressure (p_{tube}) for several blockage ratios (A_{caps}/A_{tube}) with a capsule diameter $D_{caps} = 2.7$ m. Calculations are based on eq. (16). The estimated values are based on a default pumping performance ($\dot{V}_{pump}/P_{pump}$) of 36.36 m^3/h per kW (i.e., 10.1 L/s per W) [24], [25].

(p_{atm}) and the tube pressure (p_{tube}). By inserting eq. (7), one obtains eq. (15) in terms of the blockage ratio (β), yielding

$$E_{tube} = \frac{\pi}{\beta}\left(\frac{D_{caps}}{2}\right)^2 l_{tube} \frac{\ln\left(\frac{p_{atm}}{p_{tube}}\right)}{\left(\frac{\dot{V}_{pump}}{P_{pump}}\right)}, \tag{16}$$

where the capsule diameter (D_{caps}) is the input rather than the tube diameter (D_{tube}). As shown in Fig. 10, several megawatt-hours (MWh) are needed to pressurize every kilometer of the tube. For pressures approaching one-thousand of the atmospheric pressure, the energy profile starts to get steeper. In general, the tube-operational energy needs get significantly higher when the blockage ratio gets low, opposite to the capsule's aerodynamic energy needs. This inevitably represents an optimization problem, where lowering the capsule's air resistance energy requirements will increase the tube's energy requirement instead. Moreover, it will benefit operating the tube for long periods of time since much energy is used to depressurize the tube. The way the Hyperloop tube is operated (number of capsules involved) will strongly influence the energy needs per revenue-passenger-kilometer (RPK), which is an important metric to evaluated the effectiveness of the Hyperloop transportation system (HTS). As an example, 3 MWh/km (blockage ratio of 0.3) implies 3000 MWh to depressurize a 1000 km tube. Vacuum pumps along the tube would then need 24 h of a total pumping power of 125 MW.

2) TUBE LEAKAGE COMPENSATION

Once the tube is pressurized to the desired value, one would have to maintain the pressure. According to Darcy's law (the so-called 'Ohms law for air leak'), the volumetric leakage ($\dot{V}_{leak}$) through a cylindrical porous tube (i.e., concrete is a porous medium) is proportional to the pressure drop through it [26], yielding

$$v_{leak} = \frac{\dot{V}_{leak}}{2\pi r l_{tube}} = -\frac{k}{\mu}\frac{dp}{dr}, \tag{17}$$

where k is the air permeability of the medium (concrete), μ is the dynamic viscosity of the gaseous medium (air), and r is the radial position inside the cylindrical tube wall. The mass conservation principle holds that the gradient of the mass flow rate out of the tube is zero, yielding the following.

$$\frac{d}{dr}\left(\rho \dot{V}_{leak}\right) = 0 \tag{18}$$

If one inserts of eqs. (1) and (17) into eq. (18), one obtains

$$\frac{d}{dr}\left(\frac{1}{RT} p \frac{k}{\mu}\frac{dp}{dr} 2\pi r l_{tube}\right) = \frac{d}{dr}\left(p\frac{dp}{dr} r\right) = 0, \tag{19}$$

where many terms are taken as constant along the wall thickness. Eq. (19) have inner and outer boundary conditions

$$p\left(r = \frac{D_{tube}}{2}\right) = p_{tube}, \tag{20}$$

$$p\left(r = \frac{D_{tube}}{2} + \delta\right) = p_{atm}, \tag{21}$$

respectively. Eq. (19) are first integrated respect to r, yielding

$$p\frac{dp}{dr} r = C_1, \tag{22}$$

with a general solution (obtained in the Wolfram Mathematica analytical environment)

$$p(r) = \sqrt{C_1 \ln(r) + C_2}. \tag{23}$$

The boundary conditions given in eqs. (20) and (21) are inserted in eq. (23) to replace the coefficients (C_1 and C_2). Then, the solution for $p(r)$ holds for $\frac{D_{tube}}{2} \leq r \leq \frac{D_{tube}}{2} + \delta$.

$$p(r) = \sqrt{\frac{p_{atm}^2 - p_{tube}^2}{\ln\left(1 + \frac{2\delta}{D_{tube}}\right)} \ln\left(\frac{2r}{D_{tube}}\right) + p_{tube}^2} \tag{24}$$

As a validation, insertion of the inner and the outer diameter into eq. (24) can be shown to satisfy eqs. (20) and (21). In addition, the obtained C_1 coefficient can be inserted into eq. (22) to express the pressure gradient as follows.

$$\frac{dp}{dr} = \frac{1}{pr}\frac{p_{atm}^2 - p_{tube}^2}{2\ln\left(1 + \frac{2\delta}{D_{tube}}\right)} \tag{25}$$

The leakage will be compensated by a vacuum pump at the outer boundary, which removes air from the tube. By combining eq. (25) and (17), the volumetric leakage rate at the outer diameter ($r = \frac{D_{tube}}{2} + \delta$ and $p = p_{atm}$) is found to be

$$|\dot{V}_{leak}| = \frac{\pi k l_{tube}}{\mu \ln\left(1 + \frac{2\delta}{D_{tube}}\right)}\left(\frac{p_{atm}^2 - p_{tube}^2}{p_{atm}}\right). \tag{26}$$

Alternatively, eq. (26) can be formulated in terms of the blockage ratio (β).

$$|\dot{V}_{leak}| = \frac{\pi k l_{tube}}{\mu \ln\left(1 + \frac{2\delta\sqrt{\beta}}{D_{caps}}\right)}\left(\frac{p_{atm}^2 - p_{tube}^2}{p_{atm}}\right) \tag{27}$$

The leakage is very sensitive to the permeation coefficient of concrete (k). It has been found to be in the range between

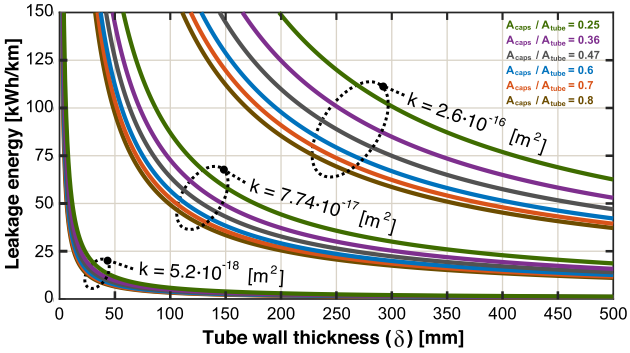

FIGURE 11. Leakage energy consumption per km per day as a function of tube concrete wall thickness (δ) for several blockage ratios (A_{caps}/A_{tube}) with a capsule diameter $D_{caps} = 2.7$ m. Calculations are based on eqs. (28) and (29), using $\mu = 1.85 \cdot 10^{-5}$ Pa · s and three different values of k [27], [28]. The estimated values are based on a default pumping performance (V_{pump}/P_{pump}) of 36.36 m^3/h per kW (i.e., 10.1 L/s per W) [24], [25].

$5.2 \cdot 10^{-18}$ m^2 and $2.6 \cdot 10^{-16}$ m^2 ("rule of thumb" says between 10^{-16} m^2 and 10^{-19} m^2) [27]. The specific estimation based on measurements was $7.74 \cdot 10^{-17}$ m^2 [28]. Moreover, since $p_{atm}^2 \gg p_{tube}^2$), the leakage can be effectively approximated by omitting the term p_{tube}^2 from eq. (27), which yields

$$|\dot{V}_{leak}| \approx \frac{\pi k l_{tube}}{\mu \ln\left(1 + \frac{2\delta\sqrt{\beta}}{D_{caps}}\right)} p_{atm}. \tag{28}$$

The leaking of air will occur for 24 hours ($\Delta t_{day} = 24$ h) every entire day the tube is depressurized, and this rate must be compensated with energy for additional depressurization (E_{leak}) per day as follows.

$$E_{leak} = \left(\frac{P_{pump}}{\dot{V}_{pump}}\right)\dot{V}_{leak}\Delta t_{day} = \frac{\dot{V}_{leak}\Delta t_{day}}{\left(\frac{\dot{V}_{pump}}{P_{pump}}\right)} \tag{29}$$

Fig. 11 indicated the leakage-of-air energy needs to be compensated per day for every kilometer, with a strong dependency on concrete's air permeability. There are also a structural requirements for the thickness, which excludes the values obtained for low wall thicknesses. Considering a perceived best case, with 2 kWh/km ($\delta = 250$ mm and $k = 5.2 \cdot 10^{-18}$ m^2) for a tube of 1000 km, one obtains an energy need of 2 MWh per day. This implies an average pumping power of 83.33 kW for a 1000 km to keep it depressurized once it is already depressurized. This power could be supplied by energy harvesting infrastructure, such as solar PV along the tube (attached on the roof), to compensate for the energy consumption.

III. HYPERLOOP SUSPENSION SYSTEMS

As outlined in the last section, the tube's vacuum-related energy needs and the aerodynamic energy consumption of the capsule are not the only performance requirements to operate the HTS. This section outlines the need for a vertical suspension method, where several solutions are explored. In this

TABLE 1. Comparison of different levitation systems for HTS.

Suspension variant	Advantages	Disadvantages	Reference
Electro-Dynamic Suspension (EDS)	• Highest achieved leviation speed, i.e., 630 km/h; • No active control needed, i.e. inherently stable; • No on-board energy is needed to sustain levitation; • Large air gap, i.e., insensitive to track imperfections;	• Capsule needs low-speed auxiliary wheeled system (WRS); • Simple EDS generates a high drag energy consumption; • Need magnetic shielding due to lack of magnetic circuit; • Need a very sophisticated track to reduce magnetic drag;	[9] [11] [36]–[42]
Electro-Magnetic Suspension (EMS)	• Technically easy to levitate at standstill or at low speed; • Simple guideway composed of ferromagnetic beams; • Laminated track yields lift-to-drag ratio ≥ 500; • Inherent guidance force from the salient magnetic circuit;	• Inherently undamped & unstable operating principle; • Requires precise monitoring to maintain levitation height; • Electromagnets on board requires energising power; • Interference requires separate guidance-control for high speeds;	[29]–[31] [34], [35] [43]–[48]
Electro-Dynamic Wheels (EDW)	• Levitation and propulsion can be achieved simultaneously; • The maximum thrust is almost independent of operating speed; • Able to ride over the guideway at low operating speeds; • The rotation of magnets causes thrust forces rather than drag;	• High mass of wheels results in high energy consumption; • Active on-board propulsion with rotary mechanical losses; • Wheels rotate at a high number of revolutions per minute; • Does not outperform alternatives in terms of efficiency;	[32] [49]–[52]
Wheel-on-Rail Suspension (WRS)	• Simplicity of design and construction with few unknowns; • The suspension is passive and independent of speed; • Can be used for low-speed suspension only;	• Cannot reach beyond 580 km/h, far below the near-sonic range; • The propulsive power requirement is too high for HTS; • Wheels are not scalable;	[53]–[55]
Air-Cushioned Suspension (ACS)	• Demonstrated at supersonic speed with low friction and drag; • The guideway can be low cost with less infrastructure; • The track is simply the bottum surface of the tube;	• High energy consumption of compressors at large air gaps; • Need to operate very near the ground, causing stability issues; • Risk of contact with the track causing enormous shear loads;	[4] [56]–[58]

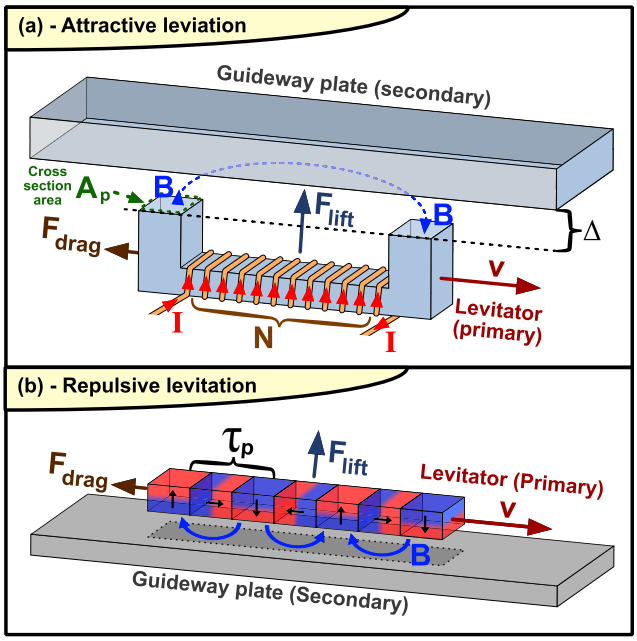

FIGURE 12. The core principle of the two main flavors of magnetic levitation is depicted (i.e., the direction of the poles can vary). a) Attractive electromagnetic levitator hanging underneath a ferromagnetic guideway. b Repulsive magnetic array levitator (lift ski) floating over a conductive guideway.

context, the suspension mechanism lifts or supports the passenger capsule to overcome its gravity to enable efficient forward motion. Examples are magnetic levitation (see Fig. 12) and air bearings that enjoy no physical contact between the track and the vehicle. As a result, the operation emits less noise, consumes less energy, and needs less maintenance, compared with "bumpy" wheel-on-rail suspension (WRS) in high-speed conditions. Moreover, it provides better ride comfort. Lateral guidance is also an essential function integrated into the vertical suspension or made as a separate subsystem. The five main categories of suspension systems are described in the following subsections, and they are depicted in Fig. 13 and summarized in Table 1.

A. ELECTRO-MAGNETIC SUSPENSION (EMS)

The electro-magnetic suspension (EMS) levitates based on the attraction force between field-wound electromagnets and ferromagnetic materials. Usually, the guideway is made of ferromagnetic iron, whereas the vehicle has active coils that control the attraction force to the iron beam [29]. This is actualized in a feedback control loop that stabilizes the levitation of the EMS. It does not need "landing" wheels because the suspension force is independent of the movement. However, at the same time, it is inherently unstable [30] and needs an active control system, which could be a point of failure. Still, the solution has a high technology readiness level ($TRL = 9$), and it is already used in Shanghai Transrapid maglev rail with an achieved speed of 430 km/h (not directly comparable to the proposed service speeds of the HTS). The lift force (F_{lift}) of an EMS pad (Fig. 12a) can be approximated as follows (assuming infinite iron permeability) [20].

$$F_{lift} \approx \frac{B^2 A}{\mu_0} = \left(\mu_0 \frac{NI}{2\Delta}\right)^2 \frac{A_p}{\mu_0} = \frac{1}{4}\mu_0 A_p N^2 \left(\frac{I}{\Delta}\right)^2 \tag{30}$$

The inputs are indicated in Fig. 12a), including pole cross-section area A_p, air gap height δ, current I and number of turns N. In addition, μ_0 is the permeability of vacuum (same as for atmospheric air). As seen, the lift is very sensitive to Δ, which implies that small air gaps are preferred (10 mm). Moreover, the force is proportional to the square of the current, which results in a significant increase in power consumption with more payloads onboard. Eq. (30) describes the stationary condition since motion induces eddy currents that can significantly deteriorate the lift (especially for non-laminated steel) [29], [31]. Eddy currents create both repulsive forces and drag forces. The lift's dependence on the motion is compensated with more current by the feedback control system, i.e., to keep the desired levitation height.

In order to combat the weakening effects of EMS, high-speed trains must be installed with laminated track iron, which greatly increases the capital costs. In these cases, the lift-to-drag ratio (or inverse of the drag-to-lift coefficient $1/c_D$) could be at least 167 [32], and in some cases beyond 500 [23]. This would imply a very low energy consumption

due to electromagnetic drag. However, EMS needs excitation power to operate its electromagnets and large currents to generate high magnetic fields, but hybrid excitation is proposed as an energy-saving strategy [33]. Moreover, by replacing the conventional electromagnet, the EMS can be configured with superconducting coils [34], [35], which can greatly improve the magnetic strength, especially at high air gap heights. Moreover, it can reduce the onboard heating of the classical coils if it can be cooled cryogenically(e.g., 77 K, or lower temperatures).

B. ELECTRO-DYNAMIC SUSPENSION (EDS)

Opposite of the EMS, repulsive forces are utilized for levitation in the electro-dynamic suspension (EDS) system. These forces are generated from a magnetic field that travels relative to a conductive material, as depicted in Fig. 12b). Magnetized lift skies are moving over a conductive track to induce eddy currents according to Faraday's and Lenz's law. The levitator can be made of either iron-free permanent magnet (PM) Halbach arrays or superconducting magnets (SCMs). The flux-concentrated Halbach arrays optimize the use of PM materials. Thus, it can save weight since no iron backing material is needed to create high flux densities. An EDS with a sinusoidal flux-distributed array moving over a conducting sheet has a lift-to-drag ratio as follows (within $\pm 10\,\%$ precision) [9].

$$\frac{F_{lift}}{F_{drag}} = \frac{1}{c_D} \approx \sqrt{\frac{\tau_p \sigma \mu_0 v}{2\pi}} \sim \sqrt{\tau_p} \cdot \sqrt{v} \tag{31}$$

In this scaling law equation, the pole pitch of the magnetic array (τ_p), the service speed (v), the lift force (F_{lift}) and the drag force (F_{drag}) are all indicated in Fig. 12b). Increasing τ_p improves the performance of the levitator. This is shown in Fig. 3, where τ_p is increased from 0.25 m to 1.0 m. In addition, it is seen that as the speed increases, the magnetic drag-to-lift reduces significantly. The magnetic drag causes levitation power to be absorbed from the vehicle's kinetic motion, which is sustained by the integrated propulsion system. The magnetic power consumption can be reduced even more, as the primitive scaling law does not consider the possibility of conductive sheet segmentation to reduce the magnetic drag force further [11], [59]. The so-called ''inductrack'' solution currently has an unknown TRL level, but it has been explored in several recent HTS feasibility projects.

A major drawback of the EDS is the fact that forward motion is required (''lift-off speed'') for the levitation mechanism to function. This implies the need for additional ''landing wheels'' to suspend the capsule under low speeds and at standstill. However, this is perceived as a minor problem considering that the EDS is simple, passively stable, fail-safe, and less expensive operating at high service speeds. In fact, it does not require active tweaking of the magnetic field to achieve stable suspension, even though the levitation height is not directly controllable. The magnetic drag gets lower at high speeds, which is completely opposite to the frictional drag of wheels or aerodynamic drag of airplanes.

An upside-down approach to EDS is to put permanent magnets on the track and install superconducting YBCO material sheets onboard the vehicle [60]. The benefit is that the reaction material is cryogenically cooled (Meissner effect); however, the track requires an expensive infrastructure.

C. ELECTRO-DYNAMIC WHEELS (EDW)

In an electro-dynamic wheel (EDW), a cylindrical PM Halbach array (typical design) is rotating to induce its field over a passive conducting surface, similar to the EDS. Then, eddy currents are generated inside the surface, and it opposes the field induced. The EDW can generate levitation and thrust forces simultaneously, which makes it different from other suspension systems. In fact, the radial magnetic array's rotation generates a forward thrust force rather than a parasitic backward drag force, as in other magnetic levitation solutions. However, it requires mechanical rotation introducing the need for a rotary motor, which causes additional mechanical losses. However, with high rotary speed applied, it can achieve high levitation-to-weight ratios. Unfortunately, no commercial activities are currently developing the EDW solution, but its merits are still being investigated. The solution has not so far been used for transportation purposes, and it has a presumed low technology readiness level (TRL).

D. WHEEL-ON-RAIL SUSPENSION (WRS)

The wheel-on-rail system (WRS) is a classic method for both propulsion and suspension. However, wheels cannot feasibly be used for subsonic or near-sonic speeds proposed in the HTS. They are seen as impractical due to frictional losses, excessive heating, centrifugal forces, and dynamic instability. The wheels experience rolling friction drag (D), which is proportional to the capsule's weight (W). This is formulated by $D_{fric} = \mu_{fric} mg$, where μ_{fric} is the rolling friction coefficient (approx. 0.01 for rubber wheels on concrete ground), m is the mass of the vehicle, and g is the gravitational acceleration constant ($9.81\ m/s^2$). Then, the propulsive power (P_{fric}) needed as a result of frictional drag can be found from $P_{fric} = D_{fric} v = \mu_{fric} mgv$, where v is the capsule's service velocity. It scales linearly with both vehicle weight and velocity. Wheels also need bearings that are not frictionless either. Also, they suffer from emissions of ''bumpy'' noise and vibration due to their sensitivity to rail imperfections. The WRS is best applied as an auxiliary low-speed system in cases where EDS is selected as the main suspension system (i.e., take-off and landing wheels).

E. AIR-CUSHIONED SUSPENSION (ACS)

Air bearings were proposed when Hyperloop was rebranded back in 2013 [4]. However, no solid background calculations were convincingly presented for this solution. The so-called air-cushioned suspension (ACS) levitates the capsule by hovering on a cushion of air that is compressed from the surroundings. It is based on the same principle as a hockey table's aerodynamic lift. The needed airflow can be generated either from a fan or by taking advantage of the

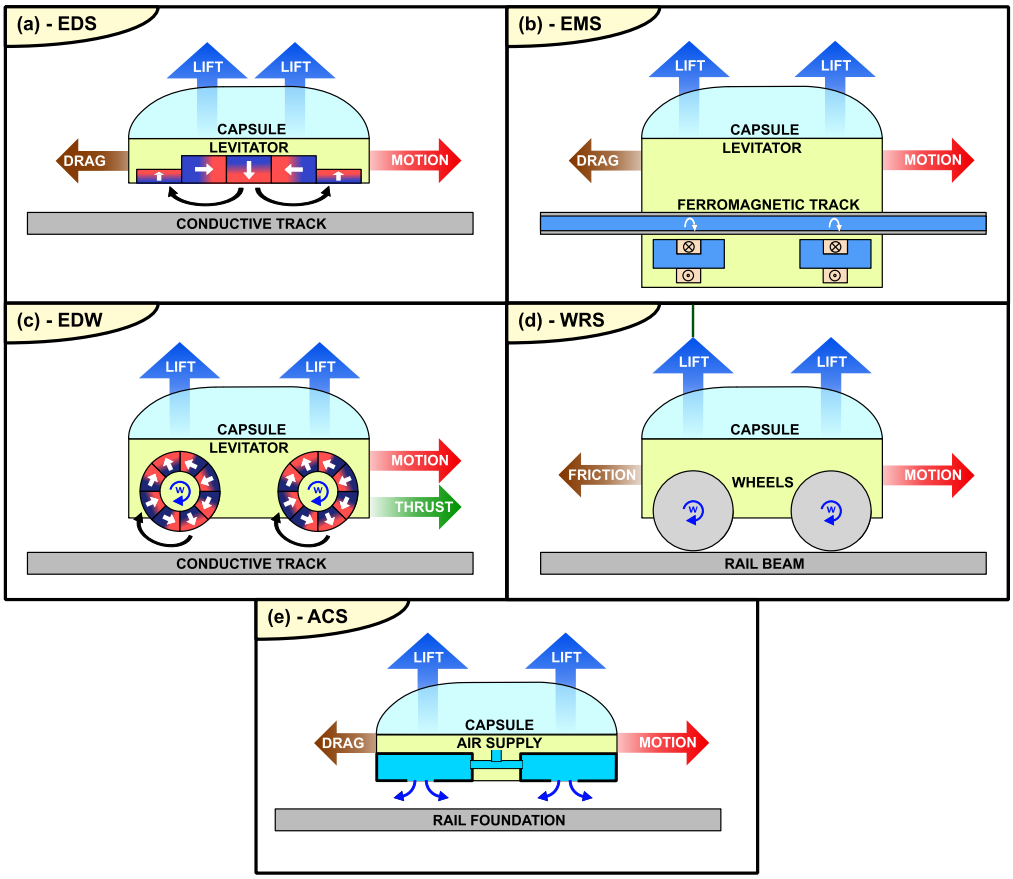

FIGURE 13. Levitation or suspension technologies fully or partially suitable for the HTS. Only core principle depicted. a) Electro-dynamic suspension (EDS). b) Electro-magnetic suspension (EMS). c) Electro-dynamic wheels (EDW). d) Wheel-on-rail suspension (WRS). e) Air-cushioned suspension (ACS).

airflow induced by the forward motion. However, in an HTS vacuum environment, a pumped mechanism is required. For short-range Hyperloop, a compressed air tank is the simplest method to supply air. However, this tank tends to become impractically huge at higher gap heights between the track and the capsule.

The most familiar concept of the ACS is found in the historical development of the tracked hovercraft (or aerotrain) in the 1960s. Large fans were blowing air underneath the hovercraft, which is prevented from escaping. The generated pressure was then able to support the weight of the vehicle. However, this principle's disadvantage was that tremendous flow rates were needed to achieve suspension heights of just a few millimeters. It is inevitable that the HTS with ACS would have to ride very closely over the track's surface. In fact, tiny irregularities on the track surface (<0.01 mm) cause drastic changes in the levitation force [61]. As a result, ACS often becomes impractical due to the large air gap length needed between the Hyperloop bogie and the track. The ACS's main parameter is the gap height since it will eventually determine the flow rate needed to operate at the standstill condition. This introduces tight manufacturing tolerances and very large energy consumptions. The air bearings' main benefit from an infrastructure perspective is that the suspension track can be just the hyperloop tube's bottom surface. However, assisting wheels are needed to rescue the vehicle if the compressor fails or if air leaks result in malfunctions. At subsonic or near-sonic speeds, this can lead to an uncomfortable and risky experience for the passengers.

In the early 1970s, many research institutions abandoned ACS since the magnetic levitation alternative would require much less power to sustain the lift force. In addition, the motors and fans needed were heavy and extremely noisy [56].

IV. HYPERLOOP PROPULSION TECHNOLOGIES

Sections II and III explored the movement and the levitation of the capsule, which both contribute to drag (e.g., aero-dynamic and magnetic). These forces have to be compensated to sustain the motion, which is the propulsion system's role. In the most likely scenario, the HTS receives electrical propulsion thrust from an integrated linear motor, which is already favored in maglev-based transportation systems [62]. This is because they can produce thrust directly without conversion from rotational energy. Their demerit is that they need at least 10 mm (i.e., more than ten times rotating machines), which make them less efficient and more loss-intensive than their rotating counterparts. Alternatively, if electro-dynamic

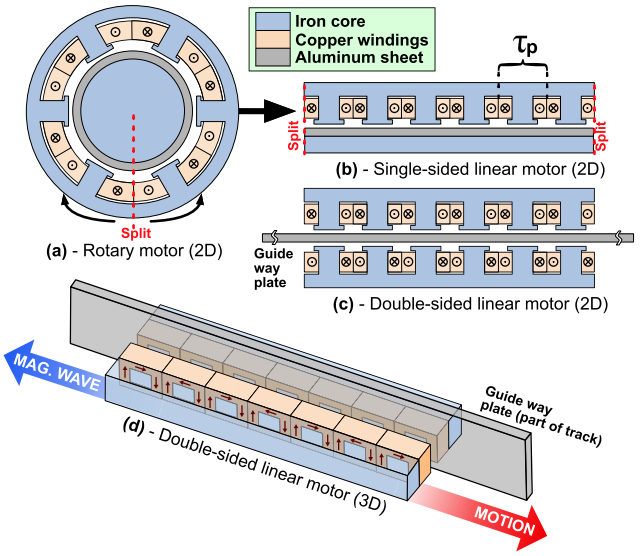

FIGURE 14. Cross-sectional view of the transformation of a rotating machine (a) to a single-sided linear motor (b). Double-sided linear motor attached to an aluminum plate indicated in (c/d).

wheels (EDW) are employed, an onboard rotating motor is installed. Either way, there is no physical contact responsible for the translational motion. In addition, wheels (WRS) may be used under low-speed operation to assist the EDS system.

Basically, the linear motor is a rotating motor that is cut open, rolled out, and installed along a guideway. This transformation is depicted in Fig. 14 for a basic induction motor, indication both single-sided and double-sided configurations. The linear motor has edge-effects that is not experienced in rotary motors. However, the core operating principle is identical. Due to higher air gap heights and end effects, energy efficiency tends to get lowered. The only commercial HTS company using the alternative rotating electric motor is Zeleros, which pursues aerodynamic propulsion. This is similar to airplanes, where rotating machines are widely applied [63]–[65].

The desired functions of the electric propulsion technology of the Hyperloop are the following.

1) Accelerate the vehicle to reach the desired cruising speed ($\geq$1000 km/h);
2) Ability to brake or de-accelerate the vehicle from the service speed ($\geq$1000 km/h). A performance benefit is regenerating of the capsule's kinetic energy;
3) Sustain the target speed between the acceleration and de-acceleration zones combating drag forces;
4) Safe magnetic field levels and comfort in the passenger compartment [66].

The maximum power capability needed is for the acceleration/de-acceleration zones [8]. After the electric propulsors have made the Hyperloop bogie reach the desired service speed, it will eventually require just a fraction of the power to maintain that speed.

The electric propulsion is generated through electromagnetic forces. The synchronous speed (v_s) of a linearly moving electromagnetic wave generated by the primary (i.e., active part) of a linear propulsion machine is

$$v_s = \frac{L}{p/2} f = 2\tau_p f, \tag{32}$$

where τ_p is the pole pitch of the armature and f is the electrical frequency [Hz]. The pole pitch is defined for the different propulsion variants in Fig. 15. The power supply frequency will directly or indirectly settle (depending on machine type) the steady-state machine velocity (v). In order to sustain the service speed, the following power ($P_{traction}$) must be supplied.

$$P_{traction} = F_{thrust} v = (F_{drag} + F_{aero}) v \tag{33}$$

Eq. (33) incorporates eq. (6) to both consider magnetic and aerodynamic drag.

$$P_{traction} = \left(mgc_D + \frac{1}{2} C_d A_{caps} \rho_{atm} \frac{p_{tube}}{p_{atm}} v^2 \right) v \tag{34}$$

In eqs. (33) and (34), F_{thrust} is the needed forward thrust force to overcome the magnetic drag (F_{drag}) and the air drag (F_{aero}), m the total mass of the vehicle, c_D (or F_{drag}/F_{lift}) the drag-to-lift ratio [predicted in eqs. (31) and (40)], C_d the aerodynamic drag coefficient of the capsule (investigated in Section II), g the acceleration of gravity (9.81 m/s^2), ρ_{atm} the atmospheric density of air (1.225 kg/m^3), p_{atm} the atmospheric pressure (101.325 kPa), p_{tube} is the pressure inside the tube environment ($\approx$101.325 Pa) and A_{caps} the frontal cross-sectional surface area of the capsule.

During the acceleration zone, additional traction power will be needed, according to

$$P_{traction} = m(a + gc_D)v + \underbrace{\frac{1}{2} C_d A_{caps} \rho_{atm} \frac{p_{tube}}{p_{atm}} v^3}_{P_{aero}}, \tag{35}$$

where a is the forward acceleration of the capsule. The primary job of the electric propulsion system (EPS) is to provide the traction power needed according to eqs. (34) and (35). The different variants of the EPS are described in in the following subsections, depicted in Fig. 15 and summarized in Table 2.

A. SHORT PRIMARY - LINEAR INDUCTION MOTOR (SP-TYPE LIM)

In the linear induction motor (LIM), a magnetic traveling wave induces eddy currents on a conducting sheet that generate a Lorentz thrust force (i.e., similar to a rotating induction motor). In the short primary (SP) version of this topology, the stator coils are onboard the vehicle, while the guideway consists of a conducting reaction beam that does not require electrification infrastructure along the track. It is very convenient and inexpensive to add aluminum material to the guideway, thus lowering the construction costs. In LIMs, the electromagnetic wave moving from the primary has a synchronous speed (v_s) that is faster than the mechanical speed (v), according to the relation

$$v = v_s(1 - s), \tag{36}$$

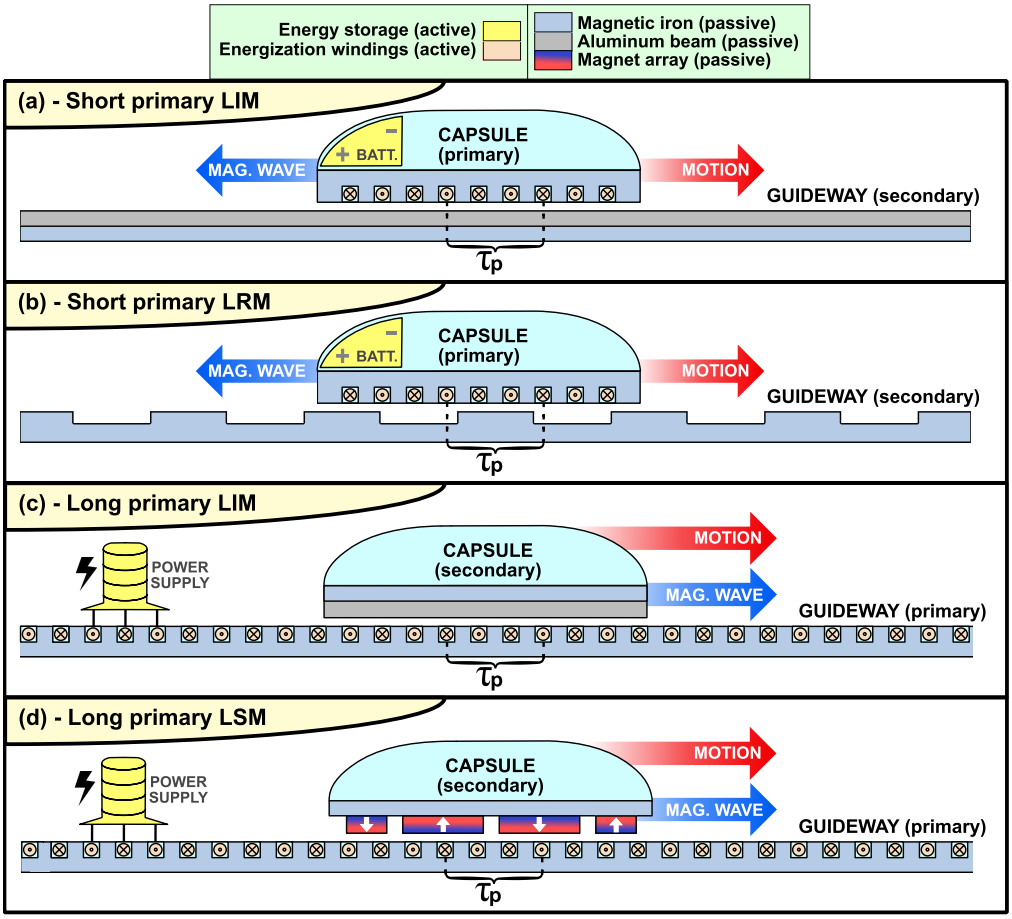

FIGURE 15. Linear EPS technologies for the HTS [Pole pitch (τ_p) is indicated, referring to eq. (32)]. a) Short primary linear induction motor (SP-LIM). b) Short primary linear reluctance motor (SP-LRM). c) Long primary linear induction motor (LP-LIM). d) Long primary linear synchronous motor (LP-LSM).

TABLE 2. Comparison of different propulsion systems for HTT.

Propulsion variant	Advantages	Disadvantages	Reference
Short Primary LIM (Linear Induction Motor)	• Relatively cheap guideway, i.e., no active parts; • A smooth and continuous thrust force is feasible;	• Requires onboard energy handled with high losses; • Short primary yields parasitic edge-field effects;	[13] [67]–[72]
Short Primary LRM (Linear Reluctance Motor)	• Has no active electrification on its guideway; • Has a relatively high energy efficiency;	• Requires onboard power at a very low power factor; • No self-starting ability & acceleration not rapid;	[73]–[75]
Long Primary LIM (Linear Induction Motor)	• Low costs & weight of the HTS capsule; • Higher speeds and lower losses than the SP-LIM;	• Expensive guideway, i.e., the track must be powered; • Low utilization of the active guideway coils;	[76]–[78]
Long Primary LSM (Linear Synchronous Motor)	• Can achieve relatively high energy efficiency; • Can achieve the highest speeds possible;	• High complexity requiring pod-station communication; • Requires very exact position recordings to function;	[12] [79]–[85]

where s is the slip. The slip is usually much higher than in rotary machines, i.e., in the range between 10 % and 20 %, which significantly reduces the maximum achievable speed (i.e., not beneficial at near-sonic speeds). This is because more induction is needed to compensate for the large air gap. This is another cause of their inefficiency since the efficiency is restricted by

$$\eta_{LIM} < 1 - s. \tag{37}$$

Due to low energy efficiency, as well as drag and edge effects, this type of topology is typically considered for low-to-medium speed maglev trains [86], such as Japanese HSST (100 km/h) [87] and Korean UTM (110 km/h) [88]. However, they are also seriously considered for super high-speed HTS because of their significantly low cost of electrification [69]. At ultra-high HTS speeds, significant kinetic energy is stored in the capsule ($0.5mv^2$). SP-LIMs can regenerate a significant amount of this energy during de-acceleration, if operated as an energy harvester [69]. However, it is important to make the harvesting compatible with the onboard storage system's maximum charging rate [8]. The SP-LIM solution can be configured as a single-sided LIM (Figs. 14b and 15a, floating over a conducting sheet and acting in the vertical direction, or using a double-sided LIM acting in the lateral direction (Fig. 14d).

B. SHORT PRIMARY - LINEAR RELUCTANCE MOTOR (SP-TYPE LRM)

The core principle of the linear reluctance motor (LRM) is primary armature coils interacting with a ferromagnetic rail

track that has salient poles, segments, or notches [73]–[75]. The vehicle's primary coils generate a magnetic traveling wave synchronized with the capsule's motion to attract the salient poles along the track continuously.

C. LONG PRIMARY - LINEAR INDUCTION MOTOR (LP-TYPE LIM)

The long primary (LP) version of the linear induction motor (LIM) has a long stator and a short rotor in classical machine terminology. It means that active stator coils are installed along the guideway while the vehicle has conducting sheets onboard. It is an inevitable fact that the construction costs are higher than for an SP-LIM alternative. The Hyperloop concept was initially introduced, proposing an LP-LIM with distributed acceleration spots rather than putting coils entirely along the whole track [4] (only a small fraction of the track length), although complexity and costs will still be high. Moreover, the main flux going through the air gap must be created by the LP coils, which causes a lot of unuseful leakages. The energy efficiency of LP-LIM is inherently low.

D. LONG PRIMARY - LINEAR SYNCHRONOUS MOTOR (LP-TYPE LSM)

In a linear synchronous motor (LSM) with a long primary (LP) active-guideway, the stationary and moving part is in magnetic synchronism. As a result, the mechanical speed (v) is equal to the synchronous speed (v_s) of the magnetic wave. Therefore, the needed pole pitch will be

$$\tau_p = \frac{v}{2f}, \tag{38}$$

if the service speed (v) and the electrical frequency (f) is already determined. It is possible to make a short primary LSM with back-to-back poles. However, the machine tends to get very heavy, which is the main reason why this type of LSM is not much proposed for transportation applications [62]. The LP-LSM needs a lot of components on the guideway instead, which saves weight and space onboard the vehicle. The propulsion power is not on board the vehicle; all of it is external. However, the minimum number of phase coils (N_c) along the total track length (L) will be

$$N_c = 3\frac{L}{\tau_p} = 6L\frac{f}{v}, \tag{39}$$

based on the pole pitch (τ_p), if a three-phase system is assumed. Even though the total active material is huge, the coils can be tailored to be stronger along different sections of the track. More power infrastructure is needed in sections where high acceleration or de-acceleration functionality is required. Such an approach will save material along with the cruising zone segments of the track, which take up the majority of the sections. Still, in principle, the entire guideway turns into a linear motor. A lot of the active components will inevitably be utilized for only a tiny fraction of the HTS route. Usually, passive PMs are placed on the vehicle, yielding a low energy capsule. The desired low air gap height is only compatible with the EMS levitation system (except in cases where superconducting magnets are used, e.g., JR-maglev MLX). Due to this fact, there is a need to reduce the influence of the dynamic coupling and interaction between the propulsion and levitation mechanisms (interplay between the EMS/LSM solution) [81], which requires continuous sensing of height and position.

V. COMPLETE ELECTROTECHNICAL SOLUTIONS

So far, Sections II-IV have presented the proposed solutions for tube infrastructure, suspension, and propulsion, respectively. They raise several discussions regarding the selected HTS technology. For instance, LP-type LSMs are the best option based on benefits such as high efficiency (η) and its compatibility with subsonic and near-sonic velocities ($\geq$1000 km/h). However, their infrastructure costs are much higher when comparing them with the SP-type LIM. Moreover, LP-LSMs are not easily integrated with the EDS levitation system, which is perceived as the optimal solution to achieve fail-safe performances at ultra-high velocities. When comparing the drag power consumption of the two main magnetic levitation solutions, their performances are similar ('Inductrack' EDS and laminated EMS). This is shown in Fig. 16, where the specific power consumption per tonne weight is investigated. The two next subsections describe two complete HTS technical solutions that are currently being pursued before more discussions and analyses are provided in this section's last subsection.

A. LCS: LIGHTWEIGHT CAPSULE SOLUTION (LP-LSM+H-EMS)

As seen in Fig. 17, the LP-LSM electric propulsion can be integrated with the hybrid excited EMS (H-EMS) levitation system. It could be configured without PMs [84], but then the field windings have to provide all the excitation for the LSM, as well the levitation force of the EMS. The H-EMS can be strategically designed to make the PMs take care of the primary suspension, whereas the current in the field windings can be used for air gap height control [33]. As already mentioned, such an approach can save energy consumption as the magnetic drag is low when the track is sufficiently laminated. A major focus for the H-EMS should be on securing the suspension's reliability, especially at subsonic and near-sonic speeds. It is a fact that Earnshaw's theorem dictates that the system is inherently unstable against vertical displacements. The small air gap heights require a very reliable and sophisticated feedback control loop, where redundancy will be needed. Moreover, the control scheme must be able to deal with track irregularities [47], and dynamic deviations that are occurring [48]. Failure of sensing or control system malfunctions can lead to serious consequences. It is essential to avoid contact between the vehicle and the track at any speed. The EMS's vulnerability to its power supply makes it more prone to failure than passively based solutions. However, hybrid solutions combining both EMS and EDS have been proposed to deal with this issue [89]. The only suspension that can avoid mechanical contact is the so-called

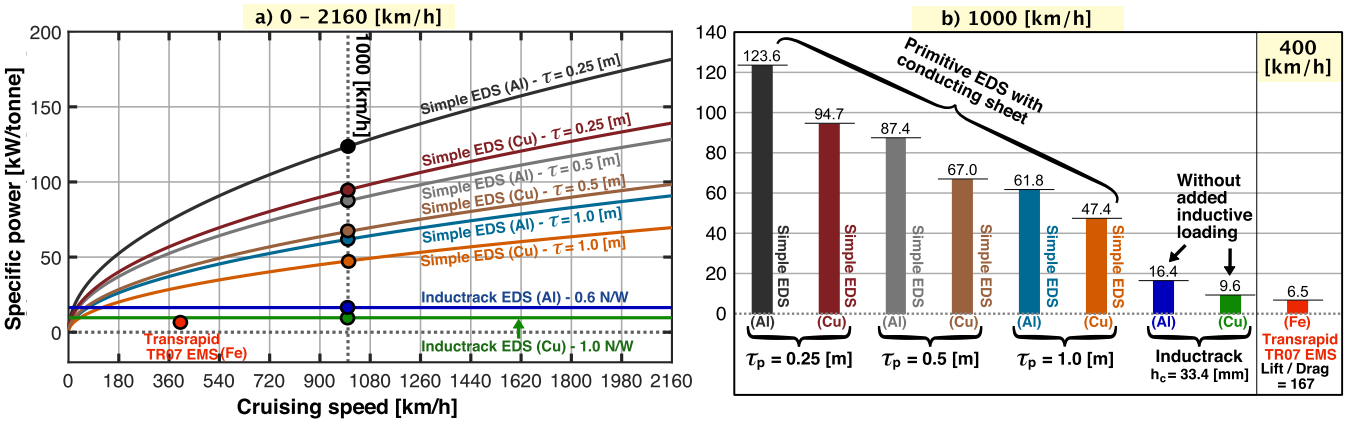

FIGURE 16. Comparison of magnetic levitation solutions, including primitive EDS [9], inductrack EDS [10], [11] and EMS [23] [Calculations based on eqs. (31), (34) & (41)]. a) Drag power consumption as a function of cruising speed. b) Comparison of drag power at 1000 km/h against laminated EMS at 400 km/h [32].

bottom-configured EMS (Fig. 2b). In this implementation, lift ski pads are installed underneath the bogie, which assists if the main levitation fails. Alternatively, the top-configured EMS 2a) would inevitably result in crashing as a result of a malfunction. This is not sufficient if a power outage happens.

Another inherent drawback of the lCS is the fact that the LP-LSM needs expensive infrastructure and power supplies along the track. However, one could plan to integrate solar panels and other renewable resources to reduce the environmental impact of the large-scale infrastructure, i.e., utilize land that is occupied better. Still, the electrification infrastructure will be incredibly expensive, and the cost must be compared against the tube infrastructure already required to enable Hyperloop technology.

B. LIS: LOW INFRASTRUCTURE SOLUTION (SP-LIM+PM-EDS)

Fig. 18 shows the SP-LIM and the 'Inductrack'-configured PM-EDS system, proposed as a robust track solution. The sub-systems are not compatible with each other, such as in the LCS. This is because the EDS air gap is too large to be efficient in combination with a LIM acting on the same surface. As a result, a double-sided LIM (DB-LIM) is functioning on a separate beam at the center of the tube. One benefit of the DB-LIM is that it has automatic lateral guidance ability, which helps it be centered [13]. This minimizes or diminishes the need for lateral guidance skies, as shown in Fig. 18. Moreover, the 'Inductrack' has the same characteristics as the primitive EDS. It is exclusively a passive configuration; thus, it lowers the cost of active infrastructure and other complications. In fact, there is no external power needed to operate the track. There are two close-packed arrays (left and right side) of inductively loaded coils. Moreover, no onboard power or levitation control circuitry is needed as well. The main challenge is that the low infrastructure solution requires an onboard power supply or contactless power transfer to sustain the electric propulsion. As a result, it depends on the availability of a sufficient energy reservoir (battery or harvesting of energy) to make it energy-autonomous [8]. However, it will effectively eliminate the need for massive amounts of power stations along the track, and thus, the construction costs outside of the capsule can be kept low. Another advantage is lowering the maintenance needs along the track, which diminishes the operational costs significantly. Moreover, it is a safety aspect that the capsule will keep levitating as long as it is moving faster than the "lift-off" speed. Its relatively large air gap height significantly lowers the probability of crashing or deviations due to track irregularities, ensuring ride comfort. If a power failure would happen, the capsule will slow down and eventually settle on its auxiliary wheels at lower speeds.

1) THE 'INDUCTRACK' SOLUTION

The 'Inductrack' PM-EDS can significantly reduce the drag power consumption, which is highlighted in Fig. 3. The expression for the lift-to-drag ratio is [11]

$$\frac{F_{lift}}{F_{drag}} = \frac{1}{c_D} = \frac{2\pi v}{\tau_p}\frac{L}{R} = Kv, \tag{40}$$

where L and R is the individual coil bundle's inductance and resistance, respectively. The pole pitch of the magnetic lift ski is τ_p. It is worth noting that if the induced current can be shifted by 90 electrical degrees, the lift-to-drag ratio can be maximized. Usually, coils of multistrand Litz wires cables are places inside each conductor bundle in the 'Inductrack' configuration. Moreover, adding more track-embedded inductive loading (L) to the levitation coils (more ferromagnetic iron) will increase the levitation's efficiency. Consequently, it is quite straightforward to adjust the R/L scaling to improve performance. For circuits without inductive loading added, the minimum performance will be [10]

$$\left(\frac{F_{lift}}{F_{drag}}\right)_{min} = \frac{1}{2}k_f \mu_0 \sigma h_c v, \tag{41}$$

which was taken into account in the plot shown in Fig. 3, assuming coil depth (h_c) of 33.4 mm, yielding a typical

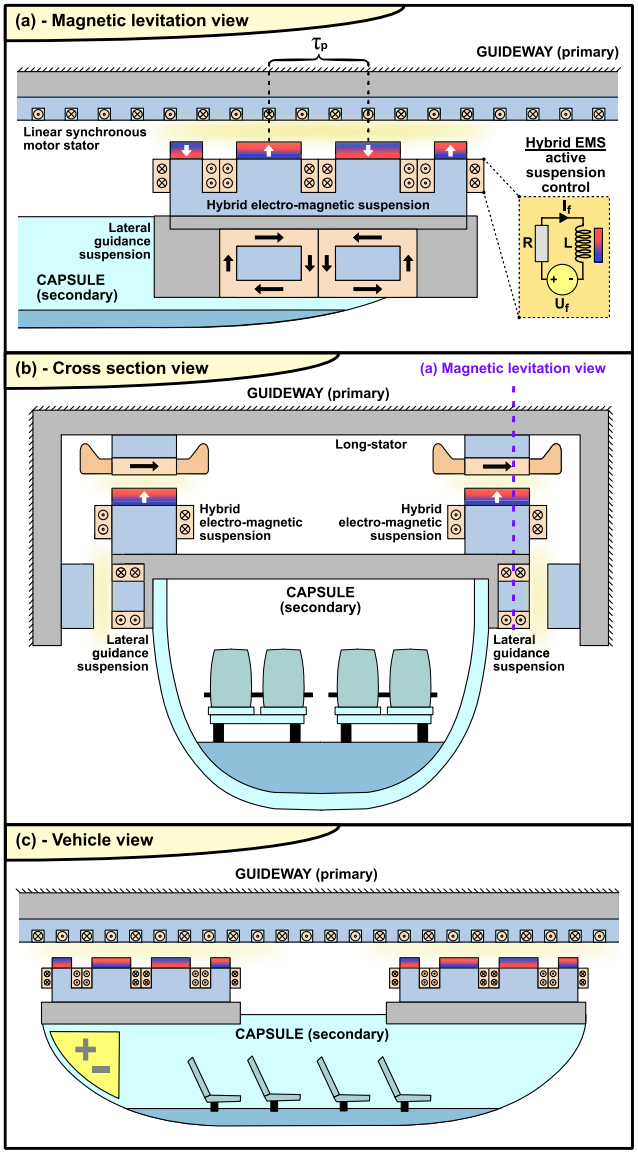

FIGURE 17. Lightweight capsule solution (LCS): A complete LP-LSM EPS and hybrid EMS levitation [33], [85], intended for the HTS with separate lateral EMS guidance. a) Magnetic levitation view. b) Cross section view. c) Vehicle view.

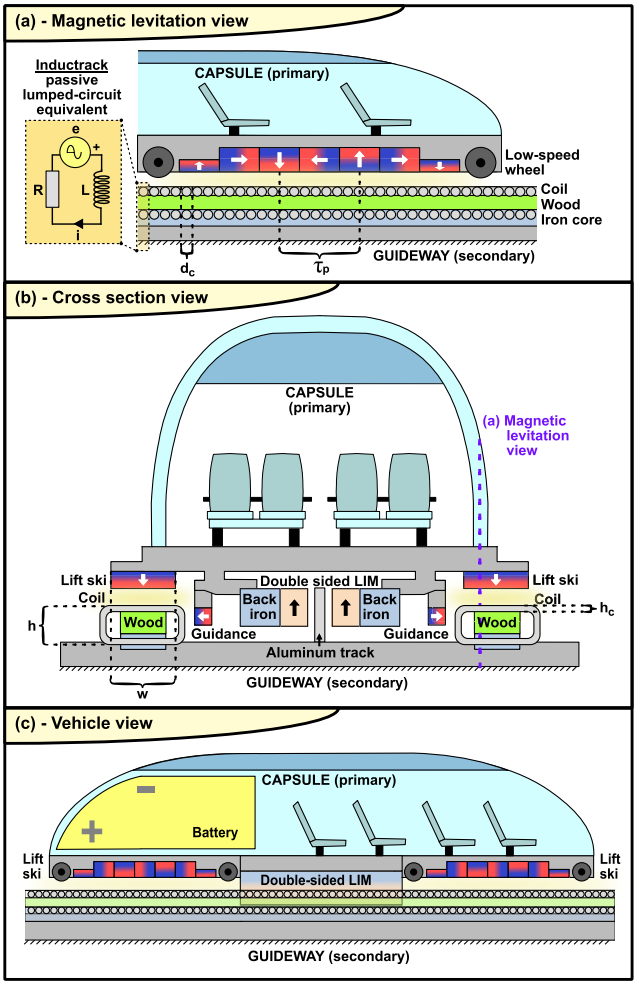

FIGURE 18. Low infrastructure solution (LIS): A complete SP-LIM EPS and EDS levitation for the HTS [9], [11], [13]. a) Magnetic levitation view. b) Cross section view [Coil depth (h_c) is indicated, referring to eq. (41)]. c) Translational view.

performance of 1 N/W [K-value in eq. (40)] lift per levitation power [11]. This advanced EDS configuration has significantly higher infrastructure costs compared with a primitive conducting beam. However, the levitation energy consumption in terms of magnetic drag becomes significantly reduced, i.e., the lift-to-drag ratio becomes approximately 278 at 1000 km/h with a very basic performance of 1 N/W.

It is worth noting that LIMs have not been in operation for high-speed transportation, even though the EDS has. From an infrastructure viewpoint, LIM combined with EDS is the preferred solution. However, the capsule's infrastructure requires heavy batteries on board, i.e., the vehicle tends to suffer from high mass and complexity.

2) RANGE PREDICTION FOR ONBOARD ENERGY RESERVOIR

The speed-profile along the track will limit the range. The maximum cruising range ($\Re_{cruise}$) of the capsule will be determined by the service speed (v) times the ratio of the available battery energy (E_{bat}), and the power is taken from the battery (P_{bat}). By also combining that $P_{traction} = \eta_{total} P_{bat}$ with eq. (34), one obtains

$$\Re_{cruise} = \frac{\eta_{tot} E'_{bat} m_{bat}}{mgc_D + \frac{1}{2} C_d A_{caps} \rho_{atm} \frac{p_{tube}}{p_{atm}} v^2}, \tag{42}$$

without considering the energy needed for acceleration of the capsule. By considering this effect, an extra of energy of $\frac{1}{2}mv^2$ must be included, yielding

$$\Re_{cruise} = \frac{\eta_{tot} E'_{bat} m_{bat} - \frac{\frac{1}{2}mv^2}{\eta_{tot}}}{mgc_D + \frac{1}{2} C_d A_{caps} \rho_{atm} \frac{p_{tube}}{p_{atm}} v^2}. \tag{43}$$

It must also be stated that taking regenerative braking into account, restoring some of the capsule's kinetic energy $\frac{1}{2}mv^2$, will not extend the range, but rather recover the energy

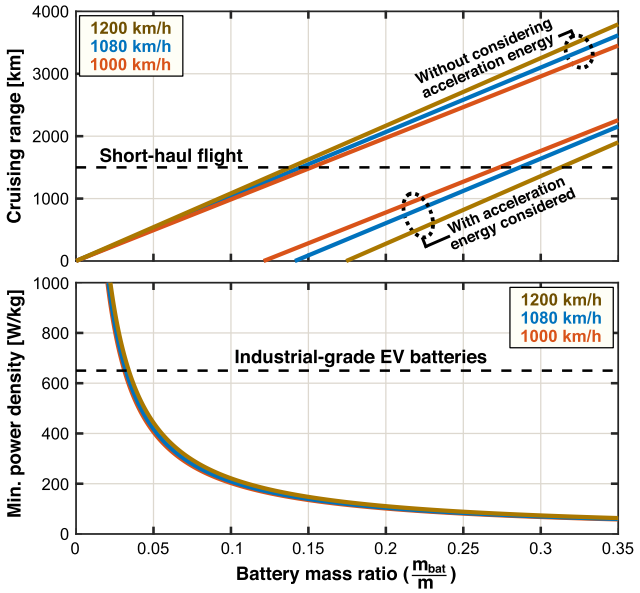

FIGURE 19. Case study of a capsule of 45 ton that has a diameter of 2.7 m ($A_{caps} = 5.726$ m^2) and is intended for 50 PAX [23]. The cruising range ($\Re_{cruise}$) and the minimum battery power density ($P'_{bat,min}$) is plotted as a function of battery mass ratio (m_{bat}/m) considered for service speeds of 1000 km/h, 1080 km/h and 1200 km/h, respectively. Calculations are based on eqs. (42) and (44). Other input data: $E'_{bat} = 200$ Wh/kg [90], $\eta_{tot} = 66.5\%$ (70% for LIM ([13]). Electromagnetic drag: K is taken as 1 N/W, where c_D was calculated using eq. (40). Aerodynamic drag: β was taken as 25%, using C_d predicted in Fig. 6 using eq. (9) [17].

for later use (improving the energy per RPK). Moreover, the minimum power density of the battery is found in cruise mode [using eq. (35)]

$$P'_{bat,min} = \frac{\left(mgc_D + \frac{1}{2}C_d A_{caps}\rho_{atm}\frac{p_{tube}}{p_{atm}}v^2\right)v}{\eta_{tot}m_{bat}}, \qquad (44)$$

which should be smaller than the actual power density (e.g., 650 kg for industrial-grade EVs [9]). This is because the acceleration power needed could be more than ten times higher than the cruising power [8], depending on the desired acceleration time.

A feasibility study of the low infrastructure solution is shown in Fig. 19, based on the work derived from all main sections of this paper and where the outputs of eqs. (42)-(44) are investigated. The prediction is made for a 45 ton, 50 PAX capsule [23]. The following can be observed if the acceleration power is taken into account. The needed battery mass should be approximately 30 % of the total mass of the capsule (slightly depending on cruising speed), including the weight of the passengers, to be compatible with short-haul flight segments (1500 km). However, if some of the kinetic energy from acceleration can be regenerated, the HTS concept's sustainability can be improved, even it does not explicitly extend the range.

C. DISCUSSION

The performance of the two referred numerical case studies of the main propulsion systems of HTS (SP-LIM and LP-LSM)

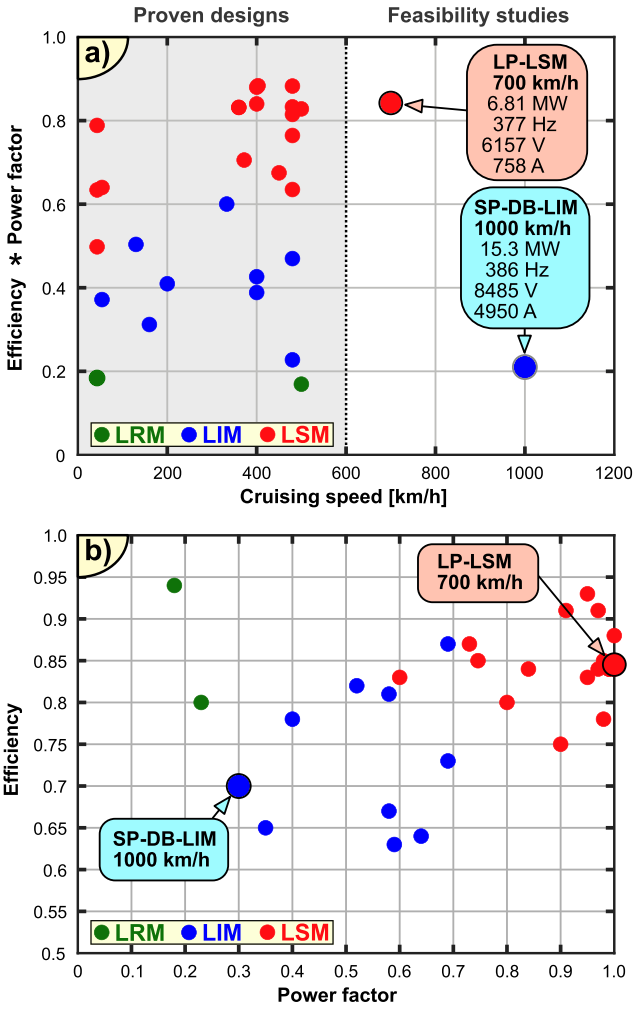

FIGURE 20. Comparison of proven LRM, LIM and LSM example designs based on worldwide project data [49], [91]. Two feasibility studies are included for cruising speeds relevant for the HTS [13], [84] [The plots refers to eq. (45)]. a) Efficiency times power factor with respect to cruising speed. b) Efficiency with respect to power factor.

are indicated in Fig. 20, which corresponds to the propulsion system for the LIS and LCS, respectively. The SP-DB-LIM was simulated for 1000 km/h cruising speed [13], whereas the LP-LSM was investigated for a speed of 700 km/h [84]. They are indicated together with commercially demonstrated maglev solutions at lower speeds to compare with existing solutions of the same machine type. It is observed that a major disadvantage with the SP-DB-LIM is a poor power factor (0.3) and a low efficiency (70 %). This results in a higher apparent power (S) with increasing inverter ratings (U and I), yielding

$$S = \sqrt{3}UI = \frac{F_{thrust}v}{\cos(\varphi)\eta_{tot}}, \qquad (45)$$

where $\cos(\varphi)$ is the power factor. The inverter onboard has to provide the reactive power, which has a detrimental effect on the inverter's power density since only 30 % of its currents contribute to the active power. It is also noted that both linear motors (SP-DB-LSM and LP-LSM) have similar performance as their counterparts in the maglev application.

TABLE 3. HTS commercial actors and their selected technologies.

Company	Country	Propulsion	Leviation	PAX	Max. speed	Reference
Zeleros	Spain	Compressed air	EMS	50	1000 km/h	[94]
Hardt Global Mobility	Netherlands	LSM (Long stator primary)	EMS (Hybrid excitation)	58	1000 km/h	[95]
Hyper Poland	Poland	-	EMS	-	1200 km/h	[96]
Hyperloop TT	USA	LSM (Long stator primary)	EDS (Inductrack)	28-50	1223 km/t	[97]
Virgin Hyperloop	USA	LIM/LSM	EDS (Inductrack)	28	1080 km/h	[98]
Transpod	Canada	LIM (Short primary)	EDS (Inductrack)	50	1000 km/h	[99]

The LP-LSM has a much higher efficiency (84 %) and power factor, but those are very sensitive to the length of each block section of the stator [92]. It must be emphasized that the feasibility studies investigating the motor performance at super-high speeds (for Hyperloop LIM and LSM) are based on evidence by numerical simulations with certain assumptions.

Both SP-LIM and LP-LSM can be configured with regenerative braking capability (generator mode). However, in the low infrastructure solution (with SP-LIM), the onboard storage's maximum charging capacity may be a limiting factor for energy harvesting [8], which hinders the possibility of an emergency stop. Moreover, if an LP-LSM is employed, the thrust capability is tailored along the track, limiting the braking and acceleration capability inside the cruising zone. Even though energy can be restored with the EPS, a fail-safe, redundant and comfortable braking functionality is required for the HTS. One effective backup solution is the passive magnetic braking, which uses the induction of eddy current on the track to slow down the vehicle. By bringing a magnetic array closer to conductive sheets on the track, the drag force will be dominating [93].

VI. CURRENT STATUS AND FUTURE NEEDS

This paper has so far gone through the main academic fields that can address the Hyperloop technology. Even though the present paper establishes the scientific basis, there are still many unanswered questions to make the technology fulfill its potential. This brief section summarizes those needs. First, the technical developments are discussed before the current need for research is outlined.

A. COMMERCIAL DEVELOPMENTS AND LIMITATIONS

The current Hyperloop technical developments worldwide rely on the work of different entrepreneurs and companies. The two main solutions described in Section V are consistent with commercial companies working with the HTS technology, summarized in Table 3. The main outsider is Zeleros, which consider rotating electric machinery for aerodynamic propulsion rather than linear electric propulsion based electromagnetic thrust.

No experiment provides strong evidence for many of the performances claimed by commercial actors. Moreover, no Hyperloop company has managed to launch a capsule in the correct environment for more than 0.5 km, i.e., there is a lack of concrete proof. All of the proposed solutions have not been tested in full scale yet, especially for long-distances and high-speeds.

B. THE NEED FOR RESEARCH

It is inevitable that the Hyperloop community currently has a weak scientific basis for their work. This is a huge opportunity for academic investigations and developments. Future research should focus on the following challenges.

1) Focus on the coordinated tube and capsule design, taking into account the strong coupling between the tube's operational energy consumption and the capsule's aerodynamic energy consumption. What is the optimal blockage ratio relating the tube size to the size of the capsule? This question builds on the foundation presented in Section II.
2) The LCS solution requires electrification infrastructure along the whole tube. This comes on top of the investments made in addressing issue 1. In order to follow the LCS technical path, one would have to show that the investment costs are small relative to the investment in the tube infrastructure, which is already quite high (i.e., this refers to issue 1).
3) What is the preferred magnetic levitation solution that balances energy consumption, infrastructure costs, and operation reliability? What is the levitation module's influence on the dynamics of the capsule? The basis for this issue is given in Sections III and V-B-1).
4) Establish experimental demonstrations of the linear induction machine (LIM) for subsonic and near-sonic speeds. How could the LIM be optimally designed to counter any side-, edge-, extremity effects, and other detrimental impacts occurring at ultra-high speeds? The current knowledge is discussed in Sections IV-A and V-C.
5) Propose a heat management approach for the low infrastructure solution (LIS). How should the propulsion losses be stored considering that the heat transfer through the tube is inefficient due to the vacuum environment? This is an additional research question that extends issue 4.
6) Develop a regenerative de-acceleration solution for the LIS technology that can handle high braking forces. How could the power electronics buffer the harvested power to make it compatible with the maximum charging rate of the energy reservoir onboard? This investigation follows the same path as issues 4, 5 and 6.

VII. CONCLUSION

The present article has comprehensively explored the Hyperloop transportation system (HTS) by analyzing its technical feasibility over various academic fields and specialities. These include aerodynamics, vacuum technology, magnetic levitation, and electric propulsion. Although no large-scale implementation has occurred yet, this paper investigates the available data, either supported by detailed numerical simulations or experimental investigations. The overall analysis provides a first-order assessment of the performance characteristics of the HTS.

The paper reviews different proposed solutions, including the integration of proposed electric propulsion systems (EPSs) and the magnetic levitation solutions. It is also discussed why different developers are favoring different solutions, based on what benefits and drawbacks they see as the most relevant features. This is the first article addressing complete electrotechnical solutions for the HTS to the best of the author's knowledge.

The article also presents the current challenges and opportunities associated with the two most promising technical solutions, i.e., the low infrastructure solution (LIS) and the lightweight capsule solution (LCS). Due to low infrastructure costs, the LIS is the most realistic option for long-distance implementations. In contrast, the LCS is best suited for near-sonic speeds (≈1235 km/h) at low energy consumption over shorter distances (due to high infrastructure investments). Even considering the higher weight and the LIS's energy-storing limitations, it is shown to be well suited for the short-haul flight (SHF) segment (1500 km). The needed energy reservoir is just a fraction of the capsule's overall mass (≈30 %), which also considers the energy needed for acceleration.

Future research items should focus on detailed-level performance investigations of the most promising options for the HTS platform. Moreover, the proposed solutions should be further investigated in terms of the cost of energy consumption under operation in light of the invested infrastructure costs. Finally, Section V outlines six key research paths that are important to establish new knowledge and potentially enable Hyperloop technology for the future.

REFERENCES

[1] E. C. Goddard, "Vacuum tube transportation system," U.S. Patent 2,511,979, Jun. 20, 1950.
[2] R. D. Thornton, "Efficient and affordable maglev opportunities in the United States," *Proc. IEEE*, vol. 97, no. 11, pp. 1901–1921, Nov. 2009.
[3] R. Palacin, "Hyperloop, the electrification of mobility, and the future of rail travel [viewpoint]," *IEEE Electrific. Mag.*, vol. 4, no. 3, pp. 4–51, Sep. 2016.
[4] E. Musk, "Hyperloop alpha," SpaceX, Hawthorne, CA, USA, Tech. Rep., 2013. [Online]. Available: https://www.tesla.com/sites/default/files/blog_images/hyperloop-alpha.pdf
[5] P. E. Ross, "Hyperloop: No pressure," *IEEE Spectr.*, vol. 53, no. 1, pp. 51–54, Jan. 2016.
[6] R. Brooks, "A few key questions can help you distinguish winners from losers," *IEEE Spectr.*, vol. 55, no. 11, pp. 46–51, Nov. 2018.
[7] K. van Goeverden, D. Milakis, M. Janic, and R. Konings, "Analysis and modelling of performances of the HL (hyperloop) transport system," *Eur. Transp. Res. Rev.*, vol. 10, no. 2, p. 41, Jun. 2018.
[8] D. Tudor and M. Paolone, "Optimal design of the propulsion system of a hyperloop capsule," *IEEE Trans. Transport. Electrific.*, vol. 5, no. 4, pp. 1406–1418, Dec. 2019.
[9] M. Flankl, T. Wellerdieck, A. Tüysüz, and J. W. Kolar, "Scaling laws for electrodynamic suspension in high-speed transportation," *IET Elect. Power Appl.*, vol. 12, no. 3, pp. 357–364, Nov. 2018.
[10] R. Post and D. Ryutov, "The inductrack concept: A new approach to magnetic levitation," Lawrence Livermore Nat. Lab., Livermore, CA, USA, Tech. Rep. UCRL-ID-124115, 1996. [Online]. Available: https://www.osti.gov/biblio/237425
[11] R. F. Post and D. D. Ryutov, "The inductrack: A simpler approach to magnetic levitation," *IEEE Trans. Appiled Supercond.*, vol. 10, no. 1, pp. 901–904, Mar. 2000.
[12] A. S. Abdelrahman, J. Sayeed, and M. Z. Youssef, "Hyperloop transportation system: Analysis, design, control, and implementation," *IEEE Trans. Ind. Electron.*, vol. 65, no. 9, pp. 7427–7436, Sep. 2018.
[13] W.-Y. Ji, G. Jeong, C.-B. Park, I.-H. Jo, and H.-W. Lee, "A study of non-symmetric double-sided linear induction motor for hyperloop all-in-one system (propulsion, levitation, and guidance)," *IEEE Trans. Magn.*, vol. 54, no. 11, pp. 1–4, Nov. 2018.
[14] J. Lim, C.-Y. Lee, S. Choi, J.-H. Lee, and K.-S. Lee, "Design optimization of a 2G HTS magnet for subsonic transportation," *IEEE Trans. Appl. Supercond.*, vol. 30, no. 4, pp. 1–5, Jun. 2020.
[15] V. Chesterton and K. Davies, "Hyperloop: Opportunity for UK supply chain," Transp. Syst. Catapult, Milton Keynes, U.K., Tech. Rep., 2018. [Online]. Available: https://ts.catapult.org.uk/news-events-gallery/news/hyperloop-opportunity-for-uk-supply-chain/ and https://s3-eu-west-1.amazonaws.com/media.ts.catapult/wp-content/uploads/2018/10/08153525/00601_Hyperloop-Report.pdf
[16] M. M. J. Opgenoord and P. C. Caplan, "Aerodynamic design of the hyperloop concept," *AIAA J.*, vol. 56, no. 11, pp. 4261–4270, Nov. 2018.
[17] J.-S. Oh, T. Kang, S. Ham, K.-S. Lee, Y.-J. Jang, H.-S. Ryou, and J. Ryu, "Numerical analysis of aerodynamic characteristics of hyperloop system," *Energies*, vol. 12, no. 3, p. 518, Feb. 2019.
[18] F. Wong, "Aerodynamic design and optimization of a hyperloop vehicle," M.S. thesis, Dept. Aerosp. Eng., Delft Univ. Technol., Delft, The Netherlands, 2018. [Online]. Available: https://repository.tudelft.nl/islandora/object/uuid%3Ab91cbd15-3f0b-4491-ae49-fdc01854927c
[19] H.-W. Lee, K.-C. Kim, and J. Lee, "Review of maglev train technologies," *IEEE Trans. Magn.*, vol. 42, no. 7, pp. 1917–1925, Jul. 2006.
[20] H.-S. Han and D.-S. Kim, *Magnetic Levitation: Maglev Technology and Applications*. New York, NY, USA: Springer, 2018.
[21] A. C. Charters and R. N. Thomas, "The aerodynamic performance of small spheres from subsonic to high supersonic velocities," *J. Aeronaut. Sci.*, vol. 12, no. 4, pp. 468–476, Oct. 1945.
[22] Rocket and Space Technology. *Basic of Space Flight: Aerodynamics*. Accessed: Jan. 5, 2021. [Online]. Available: http://www.braeunig.us/space/aerodyn_wip.htm
[23] J. K. van Leeuwen, J. M. P. Lohle, T. R. Speelman, Y. van der Tang, M. H. Teeuwen, and T. Vleeshouwer, "The future of hyperloop," Ph.D. dissertation, Dutch Ministry Infrastruct. Water Manage., Delft Univ. Technol., Delft, The Netherlands, 2019. [Online]. Available: https://drive.google.com/file/d/1TdhkxiGgjKXMnKSzqHFz6AObcCfqQLOr/view
[24] N. Yoshimura, *Vacuum Technology: Practice for Scientific Instruments*. New York, NY, USA: Springer, 2007.
[25] A. Roth, *Vacuum Technology*, 3rd ed. Amsterdam, The Netherlands: Elsevier, 2012.
[26] S. Whitaker, "Flow in porous media I: A theoretical derivation of Darcy's law," *Transp. Porous Media*, vol. 1, no. 1, pp. 3–25, 1986.
[27] T. C. Hutchinson and T. E. Soppe, "Experimentally measured permeability of uncracked and cracked concrete components," *J. Mater. Civil Eng.*, vol. 24, no. 5, pp. 548–559, May 2012.
[28] S. P. Girrens and C. R. Farrar, "Experimental assessment of air permeability in a concrete shear wall subjected to simulated seismic loading," Los Alamos Nat. Lab., Los Alamos, NM, USA, Tech. Rep LA-12124-MS and DE91 015986, 1991. [Online]. Available: https://www.osti.gov/servlets/purl/5528280
[29] J. Ding, X. Yang, Z. Long, and N. Dang, "Three-dimensional numerical analysis and optimization of electromagnetic suspension system for 200 km/h maglev train considering eddy current effect," *IEEE Access*, vol. 6, pp. 61547–61555, 2018.
[30] I. Iswanto and A. Ma'arif, "Robust integral state feedback using coefficient diagram in magnetic levitation system," *IEEE Access*, vol. 8, pp. 57003–57011, 2020.

[31] J. Du and H. Ohsaki, "Numerical analysis of eddy current in the EMS-maglev system," in *Proc. 6th Int. Conf. Electr. Mach. Syst.*, vol. 2, Nov. 2003, pp. 761–764.
[32] W. Qin and J. Z. Bird, "Electrodynamic wheel magnetic rolling resistance," *IEEE Trans. Magn.*, vol. 53, no. 8, pp. 1–7, Aug. 2017.
[33] N. Grebennikov, A. Kireev, N. Kozhemyaka, and G. Kononov, "Hybrid electromagnetic suspension for high-speed vacuum transport," *Int. J. Power Electron. Drive Syst.*, vol. 10, no. 1, p. 74, Mar. 2018.
[34] J. Xu, J. Li, G. Li, and Z. Guo, "Design and preliminary prototype test of a high temperature superconducting suspension electromagnet," *IEEE Trans. Appl. Supercond.*, vol. 25, no. 2, pp. 1–6, Apr. 2015.
[35] J. Xu, Q. Geng, Y. Li, and J. Li, "Design, fabrication, and test of an HTS magnetic suspension experimental system," *IEEE Trans. Appl. Supercond.*, vol. 26, no. 6, pp. 1–6, Sep. 2016.
[36] R. J. Hill, "Teaching electrodynamic levitation theory," *IEEE Trans. Educ.*, vol. 33, no. 4, pp. 346–354, Nov. 1990.
[37] T. Sakamoto, A. R. Eastham, and G. E. Dawson, "Induced currents and forces for the split-guideway electrodynamic levitation system," *IEEE Trans. Magn.*, vol. 27, no. 6, pp. 5004–5006, Nov. 1991.
[38] E. E. Burkhardt, J. Schwartz, and S. Nakamae, "Analysis of superconducting magnet (SCM)-ground coil interactions for EDS maglev coil configurations," *IEEE Trans. Appl. Supercond.*, vol. 3, no. 1, pp. 430–433, Mar. 1993.
[39] T. Gao, J. Yang, L. Jia, Y. Deng, W. Zhang, and Z. Zhang, "Design of new energy-efficient permanent magnetic maglev vehicle suspension system," *IEEE Access*, vol. 7, pp. 135917–135932, 2019.
[40] F. Albicini, M. Andriollo, G. Martinelli, and A. Morini, "General expressions of propulsion force in EDS-MAGLEY transport systems with superconducting coils," *IEEE Trans. Appl. Supercond.*, vol. 3, no. 1, pp. 425–429, Mar. 1993.
[41] M. Andriollo, G. Martinelli, A. Morini, and A. Scuttari, "Optimization of the winding configuration in EDS-MAGLEV trains," *IEEE Trans. Magn.*, vol. 32, no. 4, pp. 2393–2398, Jul. 1996.
[42] R. Thome, A. Radovinsky, and B. Montgomery, "EDS levitation and guidance using sheet guideways," in *Proc. 16th Int. Conf. Magnetically Levitated Syst. Linear Drives*, 2000, p. 236.
[43] Q. Chen, Y. Tan, J. Li, and I. Mareels, "Decentralized PID control design for magnetic levitation systems using extremum seeking," *IEEE Access*, vol. 6, pp. 3059–3067, 2018.
[44] S. Kusagawa, J. Baba, K. Shutoh, and E. Masada, "Multipurpose design optimization of EMS-type magnetically levitated vehicle based on genetic algorithm," *IEEE Trans. Appl. Superconduct.*, vol. 14, no. 2, pp. 1922–1925, Aug. 2004.
[45] G. Zhang, Y. Fang, F. Song, G. Zhu, and Z. Wang, "Optimal design and FEM analysis of the superconducting magnets of EMS-MAGLEV models using bi-2223 tapes," *IEEE Trans. Appiled Supercond.*, vol. 14, no. 2, pp. 1850–1853, Jun. 2004.
[46] M. Tsuchiya and H. Ohsaki, "Characteristics of electromagnetic force of EMS-type maglev vehicle using bulk superconductors," *IEEE Trans. Magn.*, vol. 36, no. 5, pp. 3683–3685, Sep. 2000.
[47] Z. Wang, Z. Long, and X. Li, "Track irregularity disturbance rejection for maglev train based on online optimization of PnP control architecture," *IEEE Access*, vol. 7, pp. 12610–12619, 2019.
[48] Y. Li, D. Zhou, P. Cui, P. Yu, Q. Chen, L. Wang, and J. Li, "Dynamic performance optimization of electromagnetic levitation system considering sensor position," *IEEE Access*, vol. 8, pp. 29446–29455, 2020.
[49] J. Bird, "An investigation into the use of electrodynamic wheels for high-speed ground transportation," Ph.D. dissertation, Dept. Elect. Comput. Eng., Univ. Wisconsin-Madison, Madison, WI, USA, 2007. [Online]. Available: https://www.researchgate.net/publication/234217871_An_investigation_into_the_use_of_electrodynamic_wheels_for_high-speed_ground_transportation
[50] J. Bird and T. A. Lipo, "Characteristics of an electrodynamic wheel using a 2-D steady-state model," *IEEE Trans. Magn.*, vol. 43, no. 8, pp. 3395–3405, Aug. 2007.
[51] J. Bird and T. A. Lipo, "A 3-D magnetic charge finite-element model of an electrodynamic wheel," *IEEE Trans. Magn.*, vol. 44, no. 2, pp. 253–265, Feb. 2008.
[52] J. Bird and T. A. Lipo, "Modeling the 3-D rotational and translational motion of a Halbach rotor above a split-sheet guideway," *IEEE Trans. Magn.*, vol. 45, no. 9, pp. 3233–3242, Sep. 2009.
[53] E. Chaidez, S. P. Bhattacharyya, and A. N. Karpetis, "Levitation methods for use in the hyperloop high-speed transportation system," *Energies*, vol. 12, no. 21, p. 4190, Nov. 2019.
[54] Y. Cheng, Z. Liu, and K. Huang, "Transient analysis of electric arc burning at insulated rail joints in high-speed railway stations based on state-space modeling," *IEEE Trans. Transport. Electrific.*, vol. 3, no. 3, pp. 750–761, Sep. 2017.
[55] C. Gong, A. Tüysüz, M. Flankl, T. Stolz, J. W. Kolar, and T. Habetler, "Experimental analysis and optimization of a contactless eddy-current-based speed sensor for smooth conductive surfaces," *IEEE Trans. Ind. Electron.*, vol. 67, no. 10, pp. 8817–8828, Oct. 2020.
[56] R. Hope, "Dropping the tracked hovercraft," *New Scientist*, vol. 57, no. 833, pp. 358–360, 1973.
[57] K. Yoshida, H. Takami, T. Yoshida, M. Suganuma, and K. Oshima, "Lateral running control for air-suspended hybrid linear motor vehicle," in *Proc. Eur. Conf. Power Electron. Appl.*, 2005, p. 9.
[58] A. Karpetis, "Fluid bearing systems and methods," U.S. Patent 10 393 175 B2, Aug. 19, 2019.
[59] R. F. Post, "Magnetic levitation system for moving objects," U.S. Patent Appl. 5 722 326, Mar. 3, 1998.
[60] Z. Deng, W. Zhang, J. Zheng, Y. Ren, D. Jiang, X. Zheng, J. Zhang, P. Gao, Q. Lin, B. Song, and C. Deng, "A high-temperature superconducting maglev ring test line developed in Chengdu, China," *IEEE Trans. Appl. Supercond.*, vol. 26, no. 6, pp. 1–8, Sep. 2016.
[61] R. Janzen, "TransPod ultra-high-speed tube transportation: Dynamics of vehicles and infrastructure," *Procedia Eng.*, vol. 199, pp. 8–17, Jan. 2017.
[62] R. Hellinger and P. Mnich, "Linear motor-powered transportation: History, present status, and future outlook," *Proc. IEEE*, vol. 97, no. 11, pp. 1892–1900, Nov. 2009.
[63] J. K. Noland, M. Leandro, J. A. Suul, and M. Molinas, "High-power machines and starter-generator topologies for more electric aircraft: A technology outlook," *IEEE Access*, vol. 8, pp. 130104–130123, 2020.
[64] M. Lukic, P. Giangrande, A. Hebala, S. Nuzzo, and M. Galea, "Review, challenges, and future developments of electric taxiing systems," *IEEE Trans. Transport. Electrific.*, vol. 5, no. 4, pp. 1441–1457, Dec. 2019.
[65] Y. Wang, S. Nuzzo, H. Zhang, W. Zhao, C. Gerada, and M. Galea, "Challenges and opportunities for wound field synchronous generators in future more electric aircraft," *IEEE Trans. Transport. Electrific.*, vol. 6, no. 4, pp. 1466–1477, Dec. 2020.
[66] R. Kircher, R. Palka, E. Fritz, K. Eiler, M. Witt, L. Blow, and J. Klühspies, "Electromagnetic fields of high-speed transportation systems. Maglev technologies in comparison with steel-wheel-rail," Assoc. Maglev Transp., Int. Maglev Board, Munich, Germany, Tech. Rep., 2018, vol. 2. [Online]. Available: https://www.researchgate.net/publication/327972538_Electromagnetic_Fields_of_High-Speed_Transportation_Systems_Maglev_Technologies_in_Comparison_ with_Steel-Wheel-Rail
[67] K. Hadziristic and V. V. Kuptsov, "Method of controlling propulsion and suspension of linear induction motors," U.S. Patent 10 476 408, Nov. 12, 2019.
[68] A. Shiri and A. Shoulaie, "Design optimization and analysis of single-sided linear induction motor, considering all phenomena," *IEEE Trans. Energy Convers.*, vol. 27, no. 2, pp. 516–525, Jun. 2012.
[69] M. Flankl, L. de Oliveira Baumann, A. Tüysüz, and J. W. Kolar, "Energy harvesting with single-sided linear induction machines featuring secondary conductive coating," *IEEE Trans. Ind. Electron.*, vol. 66, no. 6, pp. 4880–4890, Jun. 2019.
[70] P. Naderi and A. Shiri, "Modeling of ladder-secondary-linear induction machine using magnetic equivalent circuit," *IEEE Trans. Veh. Technol.*, vol. 67, no. 12, pp. 11411–11419, Dec. 2018.
[71] Q. Lu, L. Li, J. Zhan, X. Huang, and J. Cai, "Design optimization and performance investigation of novel linear induction motors with two kinds of secondaries," *IEEE Trans. Ind. Appl.*, vol. 55, no. 6, pp. 5830–5842, Nov. 2019.
[72] Y. Han, Z. Nie, J. Xu, J. Zhu, and J. Sun, "Control strategy for optimising the thrust of a high-speed six-phase linear induction motor," *IET Power Electron.*, vol. 13, no. 11, pp. 2260–2268, Aug. 2020.
[73] A. El-Antably, J. Edwards, G. Williams, P. Lindon, and P. Luke, "Steady-state performance characteristics of linear reluctance motors," *IEEE Trans. Magn.*, vol. MAG-15, no. 6, pp. 1440–1442, Nov. 1979.
[74] G. Stumberger, B. Stumberger, and D. Dolinar, "Identification of linear synchronous reluctance motor parameters," *IEEE Trans. Ind. Appl.*, vol. 40, no. 5, pp. 1317–1324, Sep. 2004.
[75] J. A. Ross, "ROMAG transportation system," *Proc. IEEE*, vol. 61, no. 5, pp. 617–620, May 1973.
[76] K. Venkataratnam and A. B. Chattopadhyay, "Analysis of electromagnetic forces in a levitated short rotor LIM. I. Finite length and finite width effects," *IEEE Trans. Energy Convers.*, vol. 17, no. 1, pp. 95–101, Mar. 2002.

[77] K. Venkataratnam and A. B. Chattopadhyay, "Analysis of electromagnetic forces in a levitated short rotor LIM. II. Lateral stabilization," *IEEE Trans. Energy Convers.*, vol. 17, no. 1, pp. 102–106, Mar. 2002.
[78] D. Hall, J. Kapinski, M. Krefta, and O. Christianson, "Transient electromechanical modeling for short secondary linear induction machines," *IEEE Trans. Energy Convers.*, vol. 23, no. 3, pp. 789–795, Sep. 2008.
[79] F. Tootoonchian and Z. Nasiri-Gheidari, "Cogging force mitigation techniques in a modular linear permanent magnet motor," *IET Electr. Power Appl.*, vol. 10, no. 7, pp. 667–674, Aug. 2016.
[80] P. C. Khong, R. Leidhold, and P. Mutschler, "Magnetic guidance of the mover in a long-primary linear motor," *IEEE Trans. Ind. Appl.*, vol. 47, no. 3, pp. 1319–1327, May 2011.
[81] J.-M. Jo, S. Y. Lee, K. Lee, Y. J. Oh, S. Y. Choi, C.-Y. Lee, and K. Lee, "A position estimator using Kalman filter with a data rejection filter for a long-stator linear synchronous motor of maglev," *IEEE Access*, vol. 8, pp. 52443–52451, 2020.
[82] P. Sen, "On linear synchronous motor (LSM) for high speed propulsion," *IEEE Trans. Magn.*, vol. 11, no. 5, pp. 1484–1486, Sep. 1975.
[83] T. Sakamoto and T. Shiromizu, "Propulsion control of superconducting linear synchronous motor vehicle," *IEEE Trans. Magn.*, vol. 33, no. 5, pp. 3460–3462, Sep. 1997.
[84] H. Lee, C. Park, and J. Lee, "Improvement of thrust force properties of linear synchronous motor for an ultra-high-speed tube train," *IEEE Trans. Magn.*, vol. 47, no. 11, pp. 4629–4634, Jun. 2011.
[85] H.-W. Cho, H.-S. Han, J.-M. Lee, B.-S. Kim, and S.-Y. Sung, "Design considerations of EM-PM hybrid levitation and propulsion device for magnetically levitated vehicle," *IEEE Trans. Magn.*, vol. 45, no. 10, pp. 4632–4635, Oct. 2009.
[86] Y. Ying, D. Jiangmin, T. Laisheng, L. Xiaochun, P. Qibiao, and Z. Wenhui, "Study on the optimization of linear induction motor traction system for fast-speed maglev train," *Transp. Syst. Technol.*, vol. 4, no. 3, pp. 156–164, 2018.
[87] Y. Yasuda, M. Fujino, M. Tanaka, and S. Ishimoto, "The first HSST maglev commercial train in Japan," in *Proc. 18th Int. Conf. Magn. Levitated Syst. Linear Drives*, 2004, pp. 76–85.
[88] D. Y. Park, B. C. Shin, and H. Han, "Korea's urban maglev program," *Proc. IEEE*, vol. 97, no. 11, pp. 1886–1891, Nov. 2009.
[89] Z. Long, G. He, and S. Xue, "Study of EDS & EMS hybrid suspension system with permanent-magnet Halbach array," *IEEE Trans. Magn.*, vol. 47, no. 12, pp. 4717–4724, Dec. 2011.
[90] M. Hepperle, "Electric flight-potential and limitations," German Aerosp. Center, Cologne, Germany, Tech. Rep. MP-AVT-209-09, 2012. [Online]. Available: https://elib.dlr.de/78726/1/MP-AVT-209-09.pdf
[91] A. Cassat and M. Jufer, "MAGLEV projects technology aspects and choices," *IEEE Trans. Appiled Supercond.*, vol. 12, no. 1, pp. 915–925, Mar. 2002.
[92] R. J. Kaye, E. Masada, and T. K. Daigaku, "Comparison of linear synchronous and induction motors: Urban maglev technology development program colorado maglev project," U.S. Federal Transit Admin., Washington, DC, USA, Tech. Rep. FTA-DC-26-7002.2004.01 SAND2004-2734P, 2004. [Online]. Available: https://www.codot.gov/programs/research/pdfs/2004/inductionmotors.pdf
[93] M. M. J. Opgenoord *et al.*, "MIT hyperloop final report," Massachusetts Inst. Technol., Cambridge, MA, USA, Tech. Rep., 2017. [Online]. Available: http://web.mit.edu/mopg/www/papers/MITHyperloop_FinalReport_2017_public.pdf
[94] *Zeleros*. Accessed: Nov. 22, 2020. [Online]. Available: https://zeleros.com/hyperloop-technology/
[95] *Hardt Global Mobility*. Accessed: Nov. 22, 2020. [Online]. Available: https://hardt.global/technology-development/
[96] *Hyper Poland*. Accessed: Nov. 22, 2020. [Online]. Available: https://www.nevomo.tech/en/
[97] *Hyperloop TT*. Accessed: Nov. 22, 2020. [Online]. Available: https://www.hyperlooptt.com/technology/
[98] *Virgin Hyperloop*. Accessed: Nov. 22, 2020. [Online]. Available: https://virginhyperloop.com
[99] *Transpod*. Accessed: Nov. 22, 2020. [Online]. Available: https://www.transpod.com/the-pod/

JONAS KRISTIANSEN NØLAND (Member, IEEE) was born in Drammen, Norway, in 1988. He received the M.Sc. degree in electric power engineering from the Chalmers University of Technology, Gothenburg, Sweden, in 2013, and the Ph.D. degree in engineering physics from Uppsala University, Uppsala, Sweden, in 2017.

Since 2018, he has been an Associate Professor with the Department of Electric Power Engineering, Norwegian University of Science and Technology (NTNU). He is currently a Scientific Advisor for the Hyperloop student initiative with NTNU (Shift Hyperloop). His current research interests include excitation systems, improved utilization of electrical machines, high-power machinery for aircraft applications, hyperloop propulsion and levitation, and transportation electrification in general.

Dr. Nøland is a member of the IEEE Transportation Electrification Community (TEC), the IEEE Industrial Electronics Society (IES), the IES Electric Machines Technical Committee, the IEEE Industry Applications Society (IAS), and the IEEE Power and Energy Society (PES). He is also a Board Member with the Norwegian Academic Committee of Publication in Technology in Electrical Power Engineering. He is also a Vice-Chair of the IEEE Power and Energy Chapter of Norway. He serves as an Editor for the IEEE TRANSACTIONS ON ENERGY CONVERSION. He serves as an Associate Editor for the IEEE TRANSACTIONS ON INDUSTRIAL ELECTRONICS.